Nuclear Physics B278 (1986) 26–60
North-Holland, Amsterdam

TESTING THE WWγ COUPLING OF THE STANDARD MODEL AT $p\bar{p}$ COLLIDERS*

Jose CORTÉS

CERN, Theory Division, CH-1211 Geneva 23, Switzerland

Kaoru HAGIWARA

DESY, Theory Group, Notkestrasse 85, D-2000 Hamburg 52, FR Germany

Franz HERZOG

Institut für Theoretische Physik, Sidlerstrasse 5, CH-3012 Berne, Switzerland

Received 6 December 1985
(Revised 21 May 1986)

The measurement of the magnetic moment μ_W of the weak boson W is crucial to test the non-abelian gauge theory of the electroweak interaction formulated by Glashow, Salam and Weinberg. We propose methods to measure μ_W at hadron colliders via the processes $p\bar{p} \to W^+\gamma X$; $W^+ \to \ell^+\bar{\nu}_\ell$ and $p\bar{p} \to W^+ X$; $W^+ \to \gamma\ell^+\bar{\nu}_\ell$. The helicity amplitudes of the parton sub-process factorizes à la Mikaelian in lowest order of the fine structure constant α, leading to peculiar angular distributions among the initial and final state particles. We make extensive numerical studies at the Tevatron collider energy $\sqrt{s} = 2$ TeV of these distributions applying experimentally feasible cuts. Furthermore we investigate the main background $p\bar{p} \to W^+$ jetX; $W^+ \to \ell^+\bar{\nu}_\ell$ where the jet fakes a single isolated photon. The effect of the finite W-width is discussed and found to be small. The sensitivity of our results to higher order QCD corrections is considered qualitatively but remains unknown quantitatively.

1. Introduction

With the successful discovery of the weak boson W at the CERN proton-antiproton ($p\bar{p}$) collider [2] an immediate question arises: Is this particle the gauge boson of the renormalizable non-abelian gauge theory proposed by Glashow, Salam and Weinberg [3] or is it a vector boson of non-gauge theories [4], also compatible with all the experiments done so far?

There are two different approaches to test gauge theories: (i) Renormalizability is their most distinctive feature and thus a theoretical prediction including higher

* This is a condensed and refined version of a series of three papers by the same authors, see ref [1].

0550-3213/86/$03.50

order corrections can be compared with experiments at a quantitative level. (ii) Gauge invariance constrains the particle couplings very strongly and therefore any observables sensitive to such couplings may provide a test of gauge theories. A very prominent example of such an observable is the magnetic moment of the W-boson,

$$\mu_{\mathrm{W}} = \frac{e}{2m_{\mathrm{W}}}(1+\kappa). \tag{1.1}$$

e denotes the magnitude of the electron charge, m_{W} the mass of the W-boson and κ is the anomalous magnetic moment [5] of the W-boson. The non-abelian gauge invariance of the theory constrains the form of the gauge boson self-couplings: For any gauge theory the value of κ is unity at tree level; higher order corrections [6] are of the order of $\alpha(=e^2/4\pi)$. For non-gauge theories its value is not constrained by any fundamental principle.

At $\mathrm{p\bar{p}}$ colliders any process involving the W-boson-photon (γ) coupling is in principle sensitive to the value of κ. At the level of proton (antiproton) constituents there are two obvious candidates for such processes:

"production" process:
$$\begin{array}{l} \mathrm{d}+\bar{\mathrm{u}} \to \mathrm{W}^- + \gamma \\ \qquad\qquad \hookrightarrow \ell^- + \bar{\nu}_\ell , \end{array} \tag{1.2}$$

"decay" process:
$$\begin{array}{l} \mathrm{d}+\bar{\mathrm{u}} \to \mathrm{W}^- \\ \qquad\qquad \hookrightarrow \gamma + \ell^- + \bar{\nu}_\ell , \end{array} \tag{1.3}$$

and their charge conjugate processes. In the following discussion we consider only processes involving W^- *.

The κ-sensitivity in the production process $\mathrm{d}+\bar{\mathrm{u}} \to \mathrm{W}^- + \gamma$ and that in the decay process $\mathrm{W}^- \to \gamma + \ell^- + \bar{\nu}_\ell$, is known to be spectacular [7] due to the occurrence of spin independent zeros [8] in the tree amplitudes: If the photon coupling is that of a renormalizable gauge theory, implying $\kappa = 1$ for the W-boson, the amplitudes $\mathcal{M}(\mathrm{d\bar{u}} \to \mathrm{W}^-\gamma)$ and $\mathcal{M}(\mathrm{W}^- \to \gamma\ell^-\bar{\nu}_\ell)$, respectively have a zero in the physical region. This κ-sensitivity leads to very distinctive features for various distributions. In $\mathrm{W}\gamma$ production this amplitude zero occurs at the partonic center-of-mass (c.m.) scattering angle $\cos\theta^*_{\mathrm{d}\gamma} = \frac{1}{3}$:

$$\mathcal{M}(\mathrm{d\bar{u}} \to \mathrm{W}^-\gamma)|_{\kappa=1} = 0 \qquad \text{at } \cos\theta^*_{\mathrm{d}\gamma} = \tfrac{1}{3}. \tag{1.4}$$

In the W radiative decay case the amplitude zero shows up in the W rest frame

* Differential cross sections involving a W^+ boson are obtained from those with W^- bosons by a CP transformation. In terms of our final state variables (see eq. (2.11)) this amounts to the following replacements: $(p_{\gamma\mathrm{T}}, y_\gamma, p_{\ell\mathrm{T}}, y_\ell, \phi_\ell) \to (p_{\gamma\mathrm{T}}, -y_\gamma, p_{\ell\mathrm{T}}, -y_\ell, \phi_\ell)$.

when the photon is anticollinear to the charged lepton:

$$\mathcal{M}(W^- \to \gamma \ell^- \bar{\nu}_\ell)|_{\kappa=1} = 0 \qquad \text{at } \cos\theta^*_{\gamma\ell} = -1. \tag{1.5}$$

For any value of κ other than the gauge theory value, $\kappa = 1$, these amplitude zeros disappear.

In this paper we make an extensive study of the "production" process (1.2) as well as of the "decay" process (1.3) in search of κ-sensitive observables: Our first concern will be to show feasible methods to actually reconstruct the above mentioned angular distributions from the observable final state, consisting typically of a high transverse momentum (p_T) isolated photon and a high p_T charged lepton with large missing transverse momentum ($\not{p}_T$) from a neutrino (ν). This is a non-trivial task since we do not know the ν longitudinal momentum in general. Furthermore we give an estimate of backgrounds from W + jet events where the jet fakes a photon, a discussion of W-finite width effects, and that of the transverse motion of the W or Wγ system.

The paper is organized as follows. In sect. 2 we present differential cross-sections for the process $p\bar{p} \to \gamma + \ell^- + \bar{\nu}_\ell +$ anything, in a minimally extended standard model with an arbitrary κ-value [5] for the W-boson. By using the narrow-width approximation for the W-propagators, the partonic subprocess can be split into the "production" process (1.2) and the "decay" process (1.3). Because of the different kinematics we shall discuss these two processes in two separate subsections: In subsect. 2.1 we present the differential cross section for $p\bar{p} \to W^-\gamma X$ followed by the decay $W^- \to \ell^-\bar{\nu}_\ell$. We propose a variable $\cos\theta^*_-$ to be used in plotting the data; this variable is constructed from the measurable photon and charged lepton momenta in such a way that it coincides with one of the two possible Wγ c.m. scattering angles. In subsect. 2.2 we show the differential cross section for $p\bar{p} \to W^-X$ followed by the radiative decay $W^- \to \gamma\ell^-\bar{\nu}_\ell$. Here we suggest using a variable $\cos\theta^*_{\gamma\ell-}$ to plot data; this quantity is again constructed from the measurable photon and charged lepton momenta in such a way that it coincides with one of the possible opening angles $\cos\theta^*_{\gamma\ell}$ allowed by the ambiguity in the neutrino longitudinal momentum. Numerical estimates at $p\bar{p}$ colliders are made for the $\cos\theta^*_-$ distribution as well as for the $\cos\theta^*_{\gamma\ell-}$ distribution and we find the κ-sensitivity in both cases to be significant. We further show that a cut in the cluster transverse mass $m_T(\gamma\ell; \bar{\nu}_\ell)$ [9] can separate "production" and "decay" processes in a simple and very effective way.

In sect. 3 we discuss the influence of the finite W-width and address the difficult question of higher order QCD correction effects. The effects of the finite W-width are found to be small in both cases. The higher order QCD corrections are expected to be small in the W radiative decay signals, since they are insensitive to nonzero transverse momentum of the W. The corrections for the Wγ production process can, however, be quite large and we propose a modification of the variable $\cos\theta^*_-$ to

include transverse motion of the Wγ system. Although we argue that this modification is necessary to control higher order corrections, only an actual evaluation of the corrections would tell us if it is sufficient or not.

In sect. 4 we discuss possible background problems to the proposed angular distributions. The most severe background comes from associated production of W and a jet [10], where the jet fakes a single isolated photon. This background is found to affect the analysis for the $\cos\theta^*$ distribution significantly, while it causes little problem in the radiative decay analysis.

In sect. 5 we summarize our findings and draw some conclusion. In the appendix we present the explicit tree-level cross section for the subprocess $d\bar{u} \to \gamma \ell^- \bar{\nu}_\ell$ without making a narrow-width approximation for intermediate W propagators.

2. The process $p\bar{p} \to \gamma \ell^- \bar{\nu}_\ell$ + anything

In the standard $SU(3)_C \times SU(2)_L \times U(1)$ model the process proton(p) + antiproton($\bar{p}$) → charged lepton(ℓ) + photon(γ) + antineutrino($\bar{\nu}_\ell$) + anything takes place via a quark-antiquark annihilation, the Drell-Yan mechanism [11]. The tree-level diagrams which contribute to the subprocess

$$q(p_1) + \bar{q}'(p_2) \to \gamma(p_\gamma) + \ell^-(p_\ell) + \bar{\nu}_\ell(p_{\bar{\nu}}); \qquad q = d, s; \qquad \bar{q}' = \bar{u}, \bar{c}, \quad (2.1)$$

are shown in fig. 1. In this equation the four-momenta of each particle are shown in parentheses.

We calculate these diagrams in a minimally extended standard model where we add an anomalous WWγ coupling term to the standard model lagrangian L_{SM}:

$$L_{\text{eff}} = L_{SM} - ie(\kappa - 1) W_\mu^\dagger W_\nu (\partial^\mu A^\nu - \partial^\nu A^\mu), \quad (2.2)$$

where W^μ and A^μ denote the W and γ field operators. The additional term in (2.2) destroys non-abelian gauge invariance, and hence renormalizability, but preserves

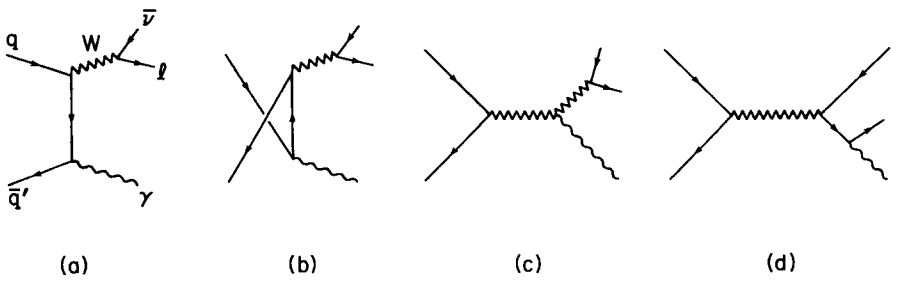

Fig. 1. Feynman diagrams which contribute to the process $q\bar{q}' \to \gamma \ell \bar{\nu}_\ell$ at tree level.

electromagnetic gauge invariance, and leads to the effective W magnetic moment (1.1)*.

The complete expression for the squared matrix element, summed (averaged) over final (initial) spin and colors is rather lengthy and is given in the appendix. In this section we will, however, discuss the process (2.1) in the narrow-width approximation for the W-boson. In this limit we can separate the process into two distinctive processes:

"production" process: $$q + \bar{q}' \to W^- + \gamma \quad \big\lfloor \to \ell^- + \bar{\nu}_\ell , \tag{2.3}$$

"decay" process: $$q + \bar{q}' \to W^- \quad \big\lfloor \to \gamma + \ell^- + \bar{\nu}_\ell . \tag{2.4}$$

The diagrams (a), (b) and (c) in fig. 1 contribute to the "production" while (c) and (d) contribute to the "decay" process.

The kinematics of these two processes is quite different: in the "production" case (2.3) the invariant mass of the lepton-pair system is equal to the W-mass m_W, i.e. $(p_\ell + p_{\bar{\nu}})^2 = m_W^2$, whereas in the radiative "decay" case (2.4) the invariant mass of the lepton-pair-photon system is given by m_W, i.e. $(p_\ell + p_{\bar{\nu}} + p_\gamma)^2 = m_W^2$. For this reason we will study these two subprocesses separately in the following two subsections.

In the QCD improved parton picture [14], the cross section for the process

$$p(P) + \bar{p}(\bar{P}) \to \gamma(p_\gamma) + \ell^-(p_\ell) + \bar{\nu}_\ell(p_{\bar{\nu}}) + X \tag{2.5}$$

can be expressed in the leading order as follows

$$d\sigma = \sum_{(a,b)} \int_0^1 d\xi \int_0^1 d\bar{\xi}\, D_{a/p}(\xi, Q^2) D_{b/\bar{p}}(\bar{\xi}, Q^2)[d\hat{\sigma}_{ab} + d\hat{\sigma}_{ba}] . \tag{2.6}$$

Here $D_{b/B}(\xi, Q^2)$ denotes the effective distribution of a parton b with the momentum fraction ξ in a hadron B at the mass-squared scale Q^2. For "production" we set $Q^2 = \hat{s}$, $\hat{s}$ being the square of the partonic c.m. energy, whereas we choose $Q^2 = m_W^2$ in the case of "decay". $d\hat{\sigma}_{ab}$ is the partonic cross section to be shown explicitly in the following subsections. $d\hat{\sigma}_{ba}$ is obtained from $d\hat{\sigma}_{ab}$ simply by exchanging the parton momenta p_a and p_b in those expressions. In the following numerical computations, we use the effective valence quark distributions parametrized by

* We do not address here the possible momentum dependence of κ nor further modifications of the effective lagrangian to include higher dimensional operators [12,13]. At present energies ($\sim m_W$) these terms should be suppressed by powers of (m_W/Λ), where Λ is the scale of compositeness.

Buras and Gaemers [15] and the effective sea-quark distribution of Owens and Reya [16].

2.1. THE PROCESS $p\bar{p} \to W^- \gamma X$; $W^- \to \ell^- \bar{\nu}_\ell$

The parton cross section for the "production" process (2.3) is expressed as

$$d\hat{\sigma}_{q\bar{q}'} = \frac{1}{2\hat{s}} \overline{\sum} |\mathcal{M}(q\bar{q}' \to W^- \gamma; W^- \to \ell^- \bar{\nu}_\ell)|^2 \, d\Phi. \tag{2.7}$$

Here $\hat{s} = (p_W + p_\gamma)^2$ and $d\Phi$ denotes the three-body phase space

$$d\Phi = (2\pi)^{-5} \delta\left[(p_q + p_{\bar{q}'} - p_\ell - p_\gamma)^2\right] \frac{d^3 p_\ell}{2E_\ell} \frac{d^3 p_\gamma}{2E_\gamma}. \tag{2.8}$$

The spin and color sum-averaged matrix element squared can be extracted from the complete formula given in the appendix; for massless quarks it reads (see eq. (A.13)):

$$\begin{aligned} &\overline{\sum} |\mathcal{M}(q\bar{q}' \to W^- \gamma; W^- \to \ell^- \bar{\nu}_\ell)|^2 \\ &\quad = \frac{128\pi^4 \alpha^2}{\sin^2\theta_W} B(W^- \to \ell^- \bar{\nu}_\ell) |U_{q'q}|^2 \delta\left[(p_q + p_{\bar{q}'} - p_\gamma)^2 - m_W^2\right] \\ &\quad \times \left\{ \left(Q_q + \frac{\hat{t}}{\hat{t} + \hat{u}} \right)^2 \frac{1}{\hat{t}\hat{u}} \left[(2p_{\bar{q}'} \cdot p_\ell)^2 + (2p_q \cdot p_\ell)^2 \right] + O(1 - \kappa) \right\}. \end{aligned} \tag{2.9}$$

θ_W denotes the Weinberg angle, $B(W^- \to \ell^- \bar{\nu}_\ell)$ the branching ratio, α the fine structure constant, $U_{q'q}$ the weak mixing matrix, Q_q the quark electric charge, $\hat{t} = (p_\gamma - p_q)^2$ and $\hat{u} = (p_\gamma - p_{\bar{q}'})^2$. The factorization [8] of the charge dependent factor is manifest in (2.9) for the $\kappa = 1$ case which leads to the amplitude zero at $\cos\theta^*_{q\gamma} = 1 + 2Q_q$ in the partonic c.m. frame. In the following we neglect both the Cabibbo rotation and the contribution from the strange and heavier quark sea. The only surviving subprocess then is $d\bar{u} \to W^- \gamma$; $W^- \to \ell^- \bar{\nu}_\ell$ with $|U_{ud}| = 1$. We set $m_W = 82$ GeV, $G_F = \pi\alpha/(\sqrt{2} \sin^2\theta_W m_W^2) = 1.17 \times 10^{-5}$ GeV^{-2} and $B(W^- \to \ell^- \bar{\nu}_\ell) = \frac{1}{12}$ for definiteness.

The cross section (2.9) depends quadratically on κ, as can be seen explicitly from (A.8). Therefore we will always plot distributions for three representative κ-values as it is enough to reconstruct distributions for arbitrary κ. We choose the κ-values $\kappa = 0, \pm 1$ for the "production" process. The cross section for an arbitrary κ-value then reads

$$d\sigma(\kappa) = \tfrac{1}{2}\kappa(1 + \kappa) \, d\sigma(1) + (1 - \kappa)(1 + \kappa) \, d\sigma(0) - \tfrac{1}{2}\kappa(1 - \kappa) \, d\sigma(-1). \tag{2.10}$$

After integrating out the azimuthal angle of the photon momentum about the beam axis we have five independent kinematical variables in terms of which the phase space factor in (2.8) can be written as

$$\frac{\mathrm{d}^3 p_\ell}{2E_\ell}\frac{\mathrm{d}^3 p_\gamma}{2E_\gamma} = \tfrac{1}{8}\pi\,\mathrm{d}p_{\ell_\mathrm{T}}^2\,\mathrm{d}y_\ell\,\mathrm{d}\phi_\ell\,\mathrm{d}p_{\gamma\mathrm{T}}^2\,\mathrm{d}y_\gamma\,. \tag{2.11}$$

Here $p_{\gamma\mathrm{T}}$ and $p_{\ell\mathrm{T}}$ denote the transverse momentum of the photon and the charged lepton with respect to the beam axis, respectively, y_γ and y_ℓ are their rapidity in the proton momentum direction, and ϕ_ℓ the azimuthal angle of $\boldsymbol{p}_{\ell\mathrm{T}}$ measured from $\boldsymbol{p}_{\gamma\mathrm{T}}$.

Shown in fig. 2a and b are the transverse momentum spectra of the photon and the charged lepton, respectively, expected at the Tevatron collider energy $\sqrt{s} = 2$ TeV. The solid line represents $\kappa = 1$, the dashed one $\kappa = 0$ and the dashed-dotted one $\kappa = -1$. The photon distribution falls strongly with rising $p_{\gamma\mathrm{T}}$; this tells us the importance of the photon identification at relatively smaller p_T values. The shape of the spectrum is mildly sensitive to κ; the steepest fall-off is expected for the gauge theory value $\kappa = 1$. On the other hand, the charged lepton p_T distribution (fig. 2b) with the cut $p_{\gamma\mathrm{T}} > 10$ GeV has a peak around $p_{\ell\mathrm{T}} = \frac{1}{2}m_\mathrm{W}$ which is a remnant of the well-known jacobian peak [17].

In fig. 3a and b we show the rapidity distribution for the photon and the charged lepton, respectively; in both figures we have imposed the cuts $p_{\gamma\mathrm{T}} > 10$ GeV and

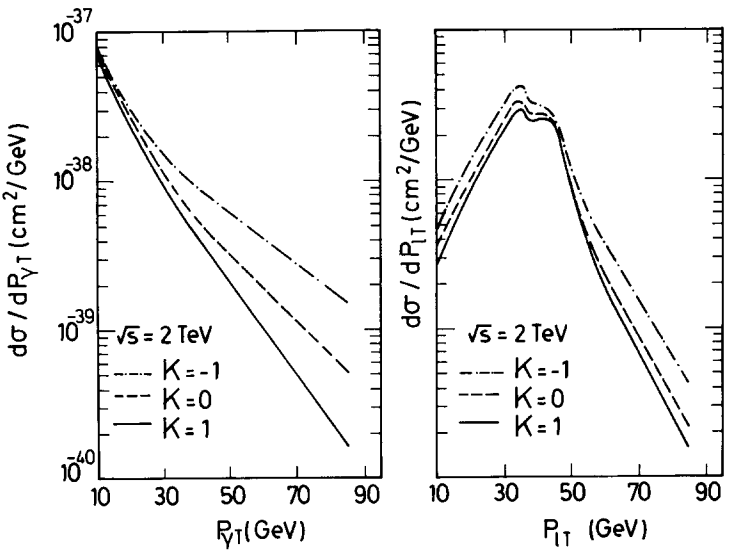

Fig. 2. The p_T distribution of the photon (a) and the charged lepton (b) in the production process $\mathrm{p\bar{p}} \to \mathrm{W}^-\gamma\mathrm{X}$; $\mathrm{W}^- \to \ell\bar{\nu}_\ell$, with cut $p_{\gamma\mathrm{T}}, p_{\ell\mathrm{T}} > 10$ GeV at $\sqrt{s} = 2$ TeV.

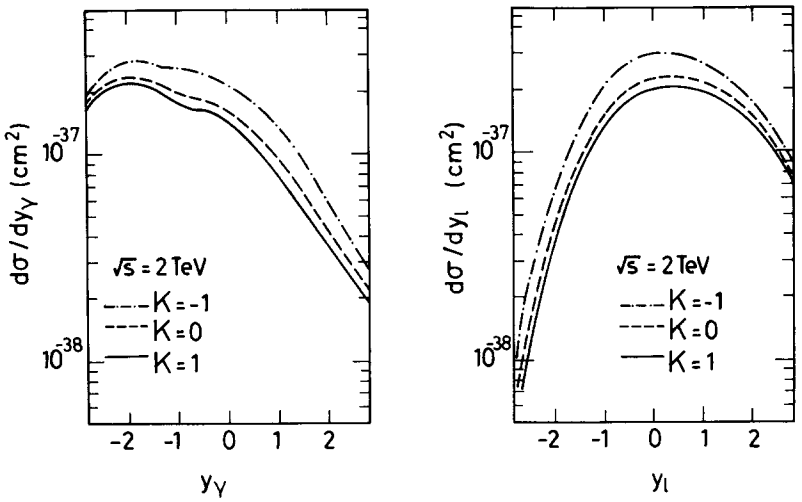

Fig. 3. The hadronic center-of-mass rapidity distribution of the photon (a) and the charged lepton (b) in the production process $p\bar{p} \to W\ \gamma X$; $W \to \ell\bar{\nu}_\ell$ with $p_{\gamma T}, p_{\ell T} > 10$ GeV. Curves below 10^{-39} cm^2/GeV are smooth interpolations of fluctuating Monte Carlo results.

$p_{\ell T} > 10$ GeV. The photon spectrum (fig. 3a) is asymmetric and has its maximum in the region of negative y_γ. This reflects the fact that the photon couples more strongly to the $\bar{u}$ quark than to the d quark and hence tends to be radiated in the $\bar{u}$, or $\bar{p}$ direction. These figures (figs. 2 and 3) show that the overall production rate grows as $|\kappa - 1|$ grows. Hence even the total rate measures κ, but with poor sensitivity. In view of the present theoretical uncertainties [18] in the precise estimate of the QCD radiative correction to the production rate, it would be desirable to look for quantities much more sensitive to the value of κ.

For the computations of the rest of this subsection we will always apply the following cuts:

$$p_{\ell T}, p_{\gamma T} > 10 \text{ GeV}; \qquad |y_\ell|, |y_\gamma| < 3. \tag{2.12}$$

These cuts are imposed to account for an actual experimental situation where one is looking for an isolated high p_T photon and a high p_T charged lepton typically with large $\not{p}_T$ (missing transverse momentum).

One of the most spectacular predictions of the electroweak gauge theory is the presence of the polarization and momentum independent angular zero in the constituent scattering amplitude for $q\bar{q}' \to W\gamma$ [7, 8]. The angular zero in the spin-average cross section disappears for non-gauge theories because only in the gauge theory case do all polarization amplitudes have a zero at the same phase space point [19]. This angular zero in the colliding parton c.m. frame is almost smeared away in the collider c.m. frame; see e.g. the γ rapidity distribution shown in fig. 3a. We need to find differential cross sections which are sensitive to κ but

relatively insensitive to the shape of the constituent distribution which is responsible for the smearing.

Since we shall discuss a dip in the cross section we should anticipate a brief discussion on the possible background problem: we are looking for events showing a high p_T charged lepton and a high p_T photon isolated from each other as well as from other hadronic activities, and large $\not{p}_T$. Apart from the photon/isolated-π^0 misidentification problem to be discussed in sect. 4, we expect many events from $W^- \to \gamma \ell^- \bar{\nu}_\ell$ decay processes; this process is interesting in itself and will be discussed in subsect. 2.2. A first guess to get rid of this background is to reject all the events where the $\gamma - \ell$ invariant mass $m_{\gamma\ell}$ is smaller than m_W. In fig. 4a we show the $m_{\gamma\ell}$ distribution of the production process (solid line) and of the W radiative decay (dashed line); both curves are for $\kappa = 1$, the standard model. If we use the cut $m_{\gamma\ell} > m_W$ to eliminate the decay process, we lose at the same time a big portion of the signal. Instead, we propose to use the cluster transverse mass m_T ($\gamma\ell$; missing), defined as follows [9]

$$m_T^2(\gamma\ell; \text{missing}) = \left[\left(m_{\gamma\ell}^2 + |\boldsymbol{p}_{\gamma T} + \boldsymbol{p}_{\ell T}|^2\right)^{1/2} + |\not{\boldsymbol{p}}_T|\right]^2 - |\boldsymbol{p}_{\gamma T} + \boldsymbol{p}_{\ell T} + \not{\boldsymbol{p}}_T|^2, \quad (2.13)$$

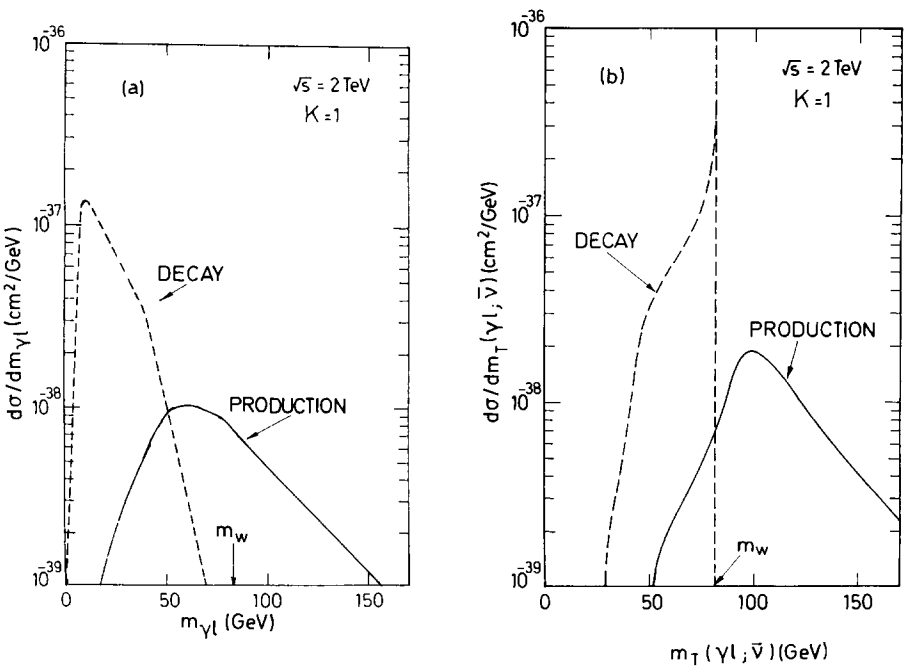

Fig. 4. The photon-lepton invariant mass distribution (a) and the cluster transverse mass distribution (b) for the production process $p\bar{p} \to W^- \gamma X$; $W^- \to \ell^- \bar{\nu}_\ell$ (solid lines) and the decay process $p\bar{p} \to W^- X$; $W^- \to \gamma \ell^- \bar{\nu}_\ell$ (dashed lines) at $\sqrt{s} = 2$ TeV. Both curves are for $\kappa = 1$ and the cuts $p_{\gamma T}, p_{\ell T} > 10$ GeV, $|y_\gamma|, |y_\ell| < 3$ and $\cos\theta_{\gamma\ell} < 0.95$ (only for decay) are implemented.

where $\not{p}_T$ denotes the missing transverse momentum vector about the beam axis. In our case there is one undetectable particle ($\bar{\nu}$) and hence $\not{p}_T = p_{\bar{\nu}T}$. In fig. 4b we plot the $m_T(\gamma\ell; \bar{\nu})$ distribution expected from the production process (solid curve) and the decay process (dashed curve); for this latter process the distribution shows the expected jacobian peak located at $m_T = m_W$. Since the cluster transverse mass is bounded by its parent mass, we only need to worry about the finite width effect and the error in the $\not{p}_T$ measurement. By accepting only those events which satisfy

$$m_T(\gamma\ell; \text{missing}) > 90 \text{ GeV}, \tag{2.14}$$

we lose only about 40% of the signal while getting rid of most contributions from the W radiative decay. In the following, we adopt the cut (2.14) as well as the cuts (2.12) in all our numerical computations of this subsection.

Let us now return to the problem of looking for the angular zero, predicted by the electroweak gauge theories [7, 8]. The angular zero appears in the Wγ c.m. frame. The problem is simply that although we can in principle measure the W transverse momentum from its leptonic decay, we cannot measure its longitudinal momentum. A typical momentum configuration for a lepton-photon-missing p_T event is shown in fig. 5 where the frame has been boosted until the lepton momentum becomes

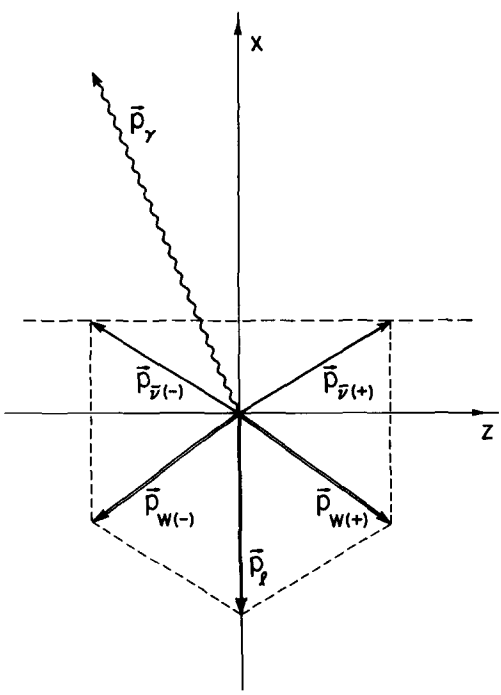

Fig. 5. Schematic view of the possible three momentum configuration of a charged lepton, a photon, a neutrino and a W in the frame where p_γ has only a negative x component. None of the three momenta but p_γ necessarily lie in the $x-z$ plane.

purely transverse. We fix the z and x axis as the proton beam and the $-\boldsymbol{p}_\ell$ direction, respectively. The dashed line shows the possible location of $\boldsymbol{p}_{\bar\nu}$ which does not necessarily lie in the $x-z$ plane for a given $\boldsymbol{p}_{\bar\nu\mathrm{T}}$. Now, it is straightforward to see that if we neglect the width of the W-boson, i.e. $\Gamma_\mathrm{W}/m_\mathrm{W}=0$, we have only two solutions for the $\bar\nu$ momentum since the invariant mass of the lepton system should form m_W. Explicitly, we have for the $\bar\nu$ rapidity

$$y_{\bar\nu(\pm)} = y_\ell \pm \ln\left\{1+\delta+\left[\delta(2+\delta)\right]^{1/2}\right\}, \tag{2.15a}$$

with

$$\delta = \max\left\{m_\mathrm{W}^2 - m_\mathrm{T}^2(\ell;\bar\nu),0\right\}/2|\boldsymbol{p}_{\ell\mathrm{T}}|\,|\boldsymbol{p}_{\bar\nu\mathrm{T}}|, \tag{2.15b}$$

$$m_\mathrm{T}^2(\ell;\bar\nu) = \left(|\boldsymbol{p}_{\ell\mathrm{T}}|+|\boldsymbol{p}_{\bar\nu\mathrm{T}}|\right)^2 - |\boldsymbol{p}_{\ell\mathrm{T}}+\boldsymbol{p}_{\bar\nu\mathrm{T}}|^2, \tag{2.15c}$$

where $m_\mathrm{T}(\ell;\bar\nu)$ is the transverse mass [9] of the $\ell\bar\nu$ system. The maximum symbol in eq. (2.15b) is required when we allow for the finite width of W (see discussions in sect. 3). We label the two solutions by $+$ and $-$, which correspond to the solutions with $y_{\bar\nu}>y_\ell$ and $y_{\bar\nu}<y_\ell$, respectively. These two solutions coincide at the maximum value of the $\ell\bar\nu$ transverse mass, $m_\mathrm{T}(\ell;\bar\nu)=m_\mathrm{W}$. Knowing the $\bar\nu$ four-momentum from (2.15), we can easily obtain the W four-momentum

$$p_{\mathrm{W}(\pm)} = p_\ell + p_{\bar\nu(\pm)}, \tag{2.16}$$

as shown in fig. 5. W bosons with these two different momenta can give exactly the same lepton momentum and $\not{p}_\mathrm{T}$. The rapidity of the Wγ system in the laboratory frame is then determined for each case by

$$\begin{aligned} y_\pm &= \tfrac{1}{2}\ln\frac{E_{\mathrm{W}(\pm)}+E_\gamma+p_{\mathrm{W}z(\pm)}+p_{\gamma z}}{E_{\mathrm{W}(\pm)}+E_\gamma-p_{\mathrm{W}z(\pm)}-p_{\gamma z}} \\ &= \tfrac{1}{2}\ln\frac{E_\ell+p_{\ell z}+E_\gamma+p_{\gamma z}+|\boldsymbol{p}_{\bar\nu\mathrm{T}}|\exp(y_{\bar\nu(\pm)})}{E_\ell-p_{\ell z}+E_\gamma-p_{\gamma z}+|\boldsymbol{p}_{\bar\nu\mathrm{T}}|\exp(-y_{\bar\nu(\pm)})}. \end{aligned} \tag{2.17}$$

It is now straightforward to obtain the photon scattering angle in the Wγ c.m. frame measured from the proton beam direction*,

$$\cos\theta^*_\pm = \tanh(y_\gamma - y_\pm). \tag{2.18}$$

* The following formula (2.18) is obtained when the Wγ system has no transverse motion about the beam axis. In an actual experiment where the Wγ system has non-zero transverse momentum, a more refined definition of the variable $\cos\theta^*_\pm$ is required to minimize the transverse momentum smearing effects. See discussions in sect. 3 and eqs. (3.3a)–(3.3c) for the possible improvements of the variable.

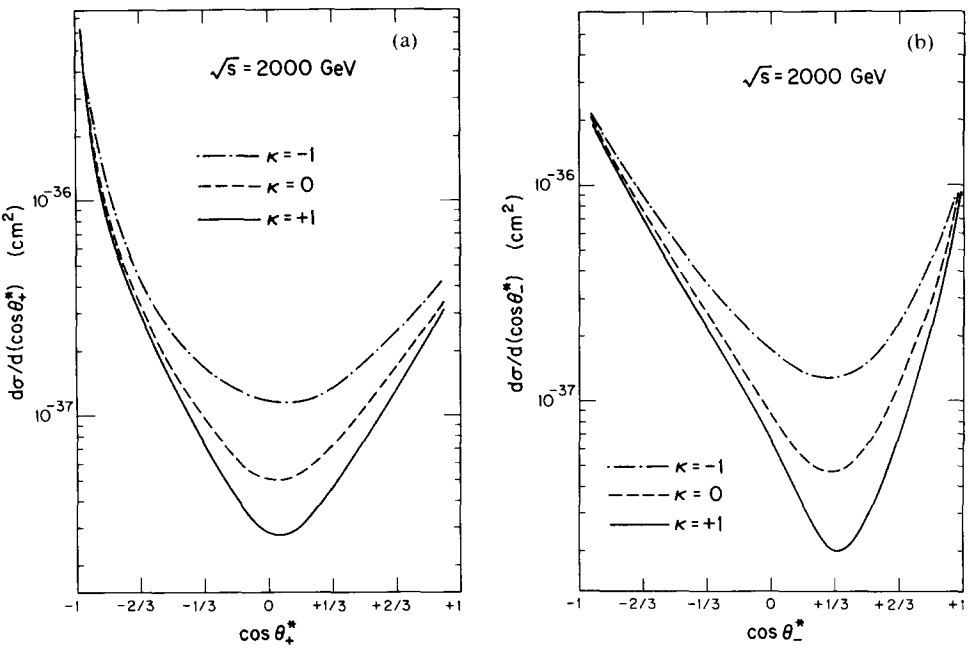

Fig. 6. The $\cos\theta^*_+$ (a) and $\cos\theta^*_-$ (b) distribution of the production process $p\bar{p} \to W^-\gamma X$; $W^- \to \ell^-\bar{\nu}_\ell$ at $\sqrt{s} = 2$ TeV. The cuts applied are specified by eqs. (2.12), (2.14). For the definition of $\cos\theta^*_\pm$ see eq. (2.18).

On an event-by-event basis we cannot tell which solution (+ or −) is actually realized. However, we may still expect the $\cos\theta^*_+$ and/or $\cos\theta^*_-$ distributions to be sensitive to the anomalous moment κ, since part of the time θ^*_+ or θ^*_- actually coincides with the true scattering angle. In fig. 6a we show our predictions for the $\cos\theta^*_+$ distribution in $p\bar{p}$ collisions at $\sqrt{s} = 2$ TeV. Although we do not have a zero, the spectrum has a minimum around $\cos\theta^*_+ = 0.1$ and its shape is rather sensitive to κ. Shown in fig. 6b are the $\cos\theta^*_-$ distribution, also at $\sqrt{s} = 2$ TeV. For $\kappa = 1$ a clean dip is seen at $\cos\theta^*_- \simeq \frac{1}{3}$. The rate difference between $\kappa = 1$ (solid curve), the gauge theory value, and $\kappa = -1$ (dashed-dotted curve) in this region is an order of magnitude; accordingly, the κ-sensitivity of the shape of the distribution is even more pronounced in the $\cos\theta^*_-$ spectrum.

The above difference between the $\cos\theta^*_+$ and the $\cos\theta^*_-$ distribution tells us that most of the time the W boson actually prefers the "−" configuration and thus the corresponding $\cos\theta^*_-$ distribution shows more similarity to the $\cos\theta^*_{d\gamma}$ distribution. Still, part of the time the W takes the "+" configuration and the zero disappears. Contributions from the subprocesses where an antiquark in p and a quark in $\bar{p}$ collide also destroy the zero but they are found to be small.

One may examine the possibility to determine κ more precisely by using a combination of the two variables, $\cos\theta^*_+$ and $\cos\theta^*_-$. One possibility [20] is to

calculate event by event the probabilities for the W to take one of the two possible configurations and to choose the higher probability solution. The problem we find in this approach is that the probability depends not only on parton distributions non-trivially but also on the matrix element squared itself, i.e. the value of κ which we want to measure. Our $\cos\theta^*_{-}$ distribution is, on the other hand a purely experimental distribution, straightforward to calculate, and shows sufficient sensitivity to κ. Its sensitivity to parton distributions enter only through a simple quantity, the relative importance of the sea-quark contribution (more precisely, the relative contribution from the subprocess where an antiquark in p and a quark in $\bar{p}$ collide). This is not too difficult to estimate quantitatively and is small anyway in $p\bar{p}$ collision at $\sqrt{s} = 2$ TeV. Hence we choose $\cos\theta^*_{-}$ as a good example of the variable whose distribution is sensitive to κ while insensitive to parton distributions.

2.2. THE PROCESS $p\bar{p} \to W^- ; W^- \to \gamma \ell^- \bar{\nu}_\ell$

The parton cross section for the "decay" process (2.4) is given by

$$d\hat{\sigma}_{q\bar{q}'} = \frac{1}{2\hat{s}} \overline{\sum} |\mathcal{M}(q\bar{q}' \to W^-; W^- \to \gamma \ell^- \bar{\nu}_\ell)|^2 \, d\Phi . \tag{2.19}$$

Here $\hat{s} = m_W^2$ and $d\Phi$ denotes the three-body phase space, eqs. (2.8) (2.11). The spin and color sum-averaged matrix element squared for an arbitrary κ is given in the appendix (eq. (A.14)). In its simplified form it reads

$$\begin{aligned} &\overline{\sum} |\mathcal{M}(q\bar{q}' \to W^-; W^- \to \gamma \ell^- \bar{\nu}_\ell)|^2 \\ &\quad = \frac{128\pi^4 \alpha^2}{\sin^2\theta_W} B(W^- \to \ell \bar{\nu}_\ell) |U_{q'q}|^2 \delta\left[(p_q + p_{\bar{q}'})^2 - m_W^2 \right] \\ &\qquad \times \left\{ \frac{(2p_\gamma \cdot p_{\bar{\nu}}) \left[(2p_{\bar{q}'} \cdot p_\ell)^2 + (2p_q \cdot p_{\bar{\nu}})^2 \right]}{(2p_\gamma \cdot p_\ell) \left[2p_\gamma \cdot (p_q + p_{\bar{q}'}) \right]^2} + O(1-\kappa) \right\} . \end{aligned} \tag{2.20}$$

As in the production case we shall neglect both the Cabibbo rotation and the contribution from the strange and heavier quark sea. The only surviving subprocess is then $d\bar{u} \to W^-$; $W^- \to \gamma \ell^- \bar{\nu}_\ell$ with $|U_{ud}| = 1$.

According to the generalized null radiation zone theorem [8], the matrix element squared (2.20) has a zero for $\kappa = 1$ when the photon and antineutrino are collinear ($p_\gamma \cdot p_{\bar{\nu}} = 0$). Although the amplitude has the same factor ($p_\gamma \cdot p_{\bar{\nu}}$) (see appendix), the cross section is linear and not quadratic in this factor because of a cancellation. This cancellation can easily be seen by comparing our result with the polarization averaged W decay distribution into a photon and a quark pair ($q\bar{q}'$)

$$W^-(p_W) \to q(p_q) + \bar{q}'(p_{\bar{q}'}) + \gamma(p_\gamma) , \tag{2.21}$$

calculated by Grose and Mikaelian [21]. The differential decay width can be expressed as

$$d\Gamma \sim \left[Q_q(p_\gamma \cdot p_{\bar{q}'}) - Q_{\bar{q}'}(p_\gamma \cdot p_q)\right]^2 \frac{(p_W \cdot p_q)^2 + (p_W \cdot p_{\bar{q}'})^2}{(p_\gamma \cdot p_q)(p_\gamma \cdot p_{\bar{q}'})}, \qquad (2.22)$$

where Q_q and $Q_{\bar{q}'}$ denote quark and antiquark charge, respectively. Notice the square of a charge dependent factor. The polarization averaged differential decay width of the process $W^- \to \gamma \ell \bar{\nu}$ can be obtained from (2.22) simply by replacing q by ℓ and $\bar{q}'$ by $\bar{\nu}$. Since $Q_{\bar{\nu}} = 0$, the charge factor in eq. (2.22) becomes simply $(p_\gamma \cdot p_{\bar{\nu}})^2$, and one of the powers is cancelled by the same factor in the denominator.

Because of this cancellation, the κ-sensitivity in the decay process is less pronounced than in the production process. We thus choose the κ-values $\kappa = -3, 1, 5$, to show our results. The cross section for an arbitrary κ-value is then obtained from the three curves via the formula

$$d\sigma(\kappa) = \tfrac{1}{32}(\kappa - 1)(\kappa + 3)\, d\sigma(5) - \tfrac{1}{16}(\kappa - 5)(\kappa + 3)\, d\sigma(1) + \tfrac{1}{32}(\kappa - 5)(\kappa - 1)\, d\sigma(-3). \qquad (2.23)$$

In the following distributions we always show separately the contribution from the production process as far as it is compatible with the cuts to be specified below. Even though this contribution may be regarded as a background in a strict sense, we add it to the signal since we find no practical way of distinguishing between these two contributions.

Shown in fig. 7a and b are the transverse momentum spectrum of the photon and the charged lepton, respectively, expected at $\sqrt{s} = 2$ TeV. The solid line represents $\kappa = 1$, the dashed one $\kappa = -3$ and the dashed-dotted one $\kappa = 5$. The following cuts have been imposed and will be applied in further distributions of this subsection:

$$p_{\gamma T},\ p_{\ell T} > 10 \text{ GeV},$$
$$|y_\gamma|,\ |y_\ell| < 3,$$
$$30 \text{ GeV} < m_T(\gamma\ell; \text{ missing}) < 90 \text{ GeV},$$
$$\cos\theta_{\gamma\ell} < 0.95. \qquad (2.24)$$

The motivation for the cut on $m_T(\gamma\ell;$ missing) was given in subsect. 2.1; the cut on the photon/charged-lepton opening angle in the collider c.m. frame is made to avoid the mass singularity. From these figures we find that the p_T distributions are governed mainly by the kinematics of the W decay and are insensitive to κ. The

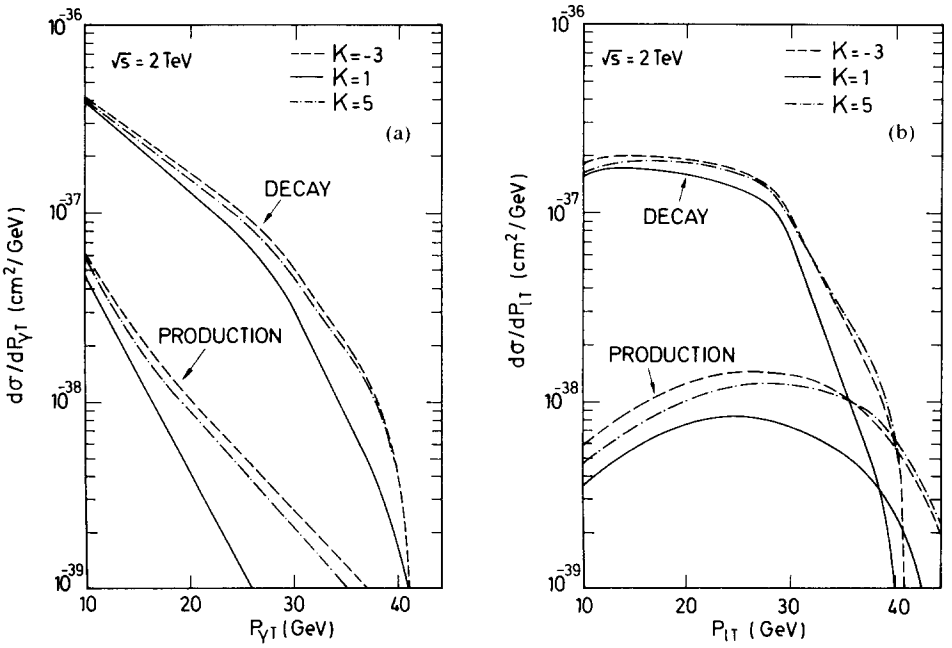

Fig. 7. The p_T distributions of the photon (a) and the charged lepton (b) in the kinematical region $m_T(\gamma\ell;\bar{\nu}) < 90$ GeV at $\sqrt{s} = 2$ TeV. Contributions from "production" and "decay" subprocesses are shown separately. The final state cuts are specified in eq. (2.24).

photon p_T distribution falls off steeply with rising p_T and thus the photon identification at relatively small p_T values (~ 10 GeV) is essential to gain statistics. On the other hand, we expect a rather flat p_T distribution for the charged lepton up to $p_T \sim 30$ GeV.

We show in fig. 8a and b the rapidity distributions of the photon and the charged lepton, respectively. Again, we see little sensitivity to κ. A clear difference between these rapidity distributions and those in the production region (see fig. 3) is that here the rapidity distributions are more or less symmetrical about the $y = 0$ axis. It is, however, obvious that we cannot determine the κ-value from these distributions: We should look for those distributions whose *shapes* are sensitive to κ.

To attack this problem we study first the final state configurations in the W rest frame. The polarization averaged W decay distribution can be expressed conveniently in terms of two variables; the photon momentum fraction

$$x = 2p_W \cdot p_\gamma / p_W^2 = 2E_\gamma^*/m_W \tag{2.25}$$

and $\cos\theta_{\gamma\ell}^*$. Here the superscript * refers to the W rest frame. For arbitrary κ the

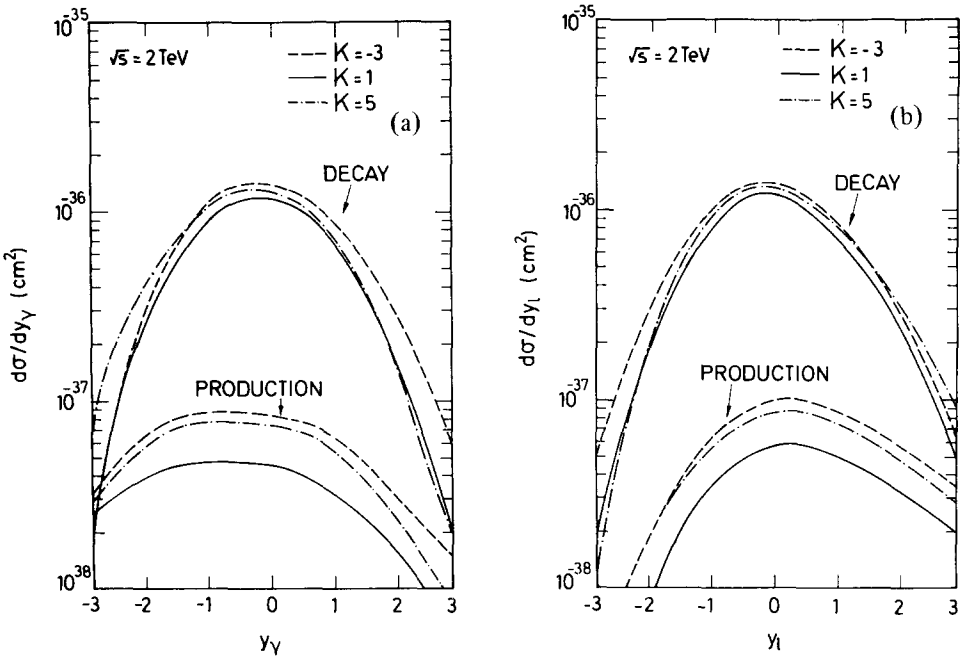

Fig. 8. The hadronic c.m. rapidity distributions of the photon (a) and the charged lepton (b) in the kinematical region $m_T(\gamma\ell,\bar{\nu}) < 90$ GeV at $\sqrt{s} = 2$ TeV. Contributions from "production" and "decay" subprocesses are shown separately. The final state cuts are specified in eq. (2.24).

normalized decay distribution reads

$$\frac{1}{\Gamma(W\to\ell\bar{\nu})}\frac{d\Gamma}{dx\,d\cos\theta^*_{\gamma\ell}} = \frac{\alpha}{4\pi}\frac{x(1-x)}{\left[1-\frac{1}{2}(1-\cos\theta^*_{\gamma\ell})x\right]^2}\sum(x,\cos\theta^*_{\gamma\ell}), \quad (2.26a)$$

with

$$\sum(x,c) = \frac{1+c}{1-c}\left[\frac{1+(1-x)^2}{x^2(1-x)} - \frac{1-c^2}{2\left(1-\frac{1}{2}(1-c)x\right)^2}\right]$$

$$+(1-\kappa)\frac{(1+c)\left(c+\frac{1}{2}(1-c)x\right)}{2\left(1-\frac{1}{2}(1-c)x\right)^2}$$

$$+\tfrac{1}{8}(1-\kappa)^2(1-x)\left[1+\frac{(1-c^2)(1+x)}{2\left(1-\frac{1}{2}(1-c)x\right)^2}\right]. \quad (2.26b)$$

The distribution (2.26b) has a single zero at $c = \cos\theta^*_{\gamma\ell} = -1$, only when $\kappa = 1$.

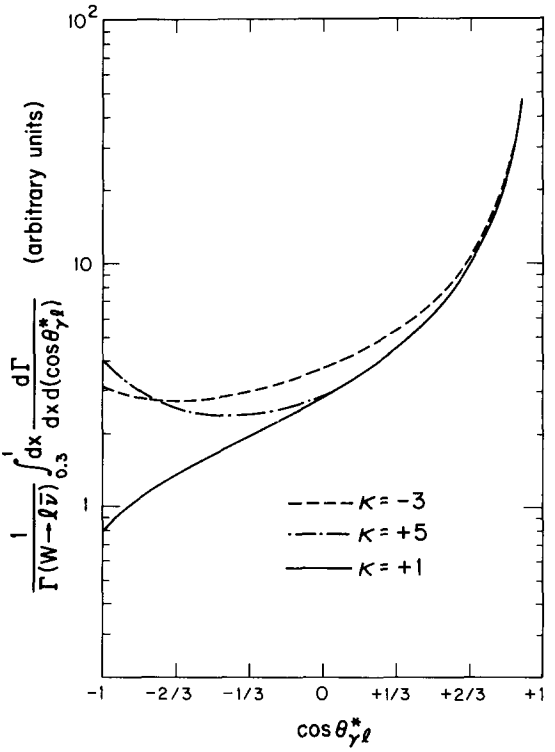

Fig. 9. The polarization averaged differential W decay distribution integrated over the region $0.3 < x < 1.0$ ($x = 2E^*_\gamma/m_W$) plotted against $\cos\theta^*_{\gamma\ell}$ in the W rest frame.

Since any deviation from the gauge theory value of κ results in filling up this zero, the $\cos\theta^*_{\gamma\ell}$ distribution is expected to be sensitive to κ.

We show in fig. 9 the $\cos\theta^*_{\gamma\ell}$ distribution integrated over the x-range $0.3 < x < 1$, a typical momentum fraction region of the photon in our analysis ($p_{\gamma T} > 10$ GeV eliminates every event with $x < 0.24$). Indeed, we find that the distribution is rather sensitive to κ in the smaller $\cos\theta^*_{\gamma\ell}$ region. However, the κ-sensitivity is weaker than that found in the angular distribution of the Wγ production process. This is partly because the distribution (2.26) has only a single zero instead of a double zero at $\kappa = 1$; we further find that the jacobian factor $(1 - \frac{1}{2}x(1 - \cos\theta^*_{\gamma\ell}))^{-2}$ plays an important role in partially compensating for the dip at $\cos\theta^*_{\gamma\ell} = -1$. This jacobian factor is responsible for the non-observability of the dip for $\kappa = 1$ and also for the enhancement observed in this region for non-gauge theory cases. Our primary goal is now to find a measurable quantity in the $p\bar{p}$ collision which is appropriate to determine κ.

An immediate candidate is the distribution in terms of the azimuthal angle $\phi_{\gamma\ell}$ between the photon and the charged lepton which is boost invariant. When

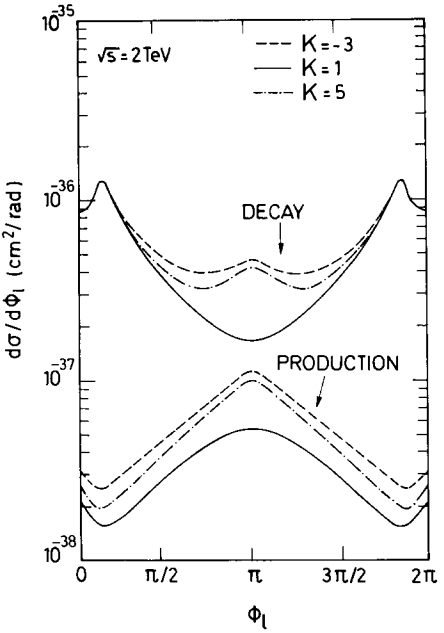

Fig. 10. Azimuthal angle $\phi_{\gamma\ell}(\measuredangle(\boldsymbol{p}_{\gamma T}, \boldsymbol{p}_{\ell T}))$ distribution at $\sqrt{s} = 2$ TeV in the kinematical region $m_T(\gamma\ell; \bar{\nu}) < 90$ GeV. Same specifications as in fig. 7. The distributions are symmetric about $\phi_{\gamma\ell} = \pi$ in our approximation.

$\cos\theta^*_{\gamma\ell} = -1$, $\phi_{\gamma\ell}$ should be π although the converse statement does not hold. Shown in fig. 10 are the expected distributions for the three κ-values. The distributions are symmetric about $\phi_{\gamma\ell} = \pi$ because of the absence of both the *CP*-violation phase and the final state interaction phase. Although there is no angular zero in this distribution, the κ-dependence of the spectrum around $\phi_{\gamma\ell} = \pi$ follows qualitatively that of the $\cos\theta^*_{\gamma\ell}$ distribution shown in fig. 9. The two peaks at $\phi_{\gamma\ell} = 18°$ and $162°$ are simply due to the collinear singularity cut, $\cos\theta_{\gamma\ell} < 0.95$ (see eq. (2.24)). This distribution may, however, suffer from a large QCD correction (see discussions in sect. 3) since the azimuthal angle is not invariant under the *transverse* motion of W. It is therefore desirable to look for a variable which refers to the W-boson rest frame.

Just as in the case of the W production process studied in the previous subsection, there is a two-fold ambiguity in the longitudinal momentum of $\bar{\nu}$. In fig. 11 we show the possible three-momentum configuration of the $\gamma\ell\bar{\nu}$ final state in the boosted frame where $\boldsymbol{p}_\ell + \boldsymbol{p}_\gamma$ has no longitudinal component. The dashed line shows the possible location of $\boldsymbol{p}_{\bar{\nu}}$ for a given $\boldsymbol{p}_{\bar{\nu}T}$.

In the limit $\Gamma_W/m_W \to 0$ the neutrino momentum is determined up to two symmetric configurations shown in the figure by $\boldsymbol{p}_{\bar{\nu}}$. Explicitly we find for the $\bar{\nu}$

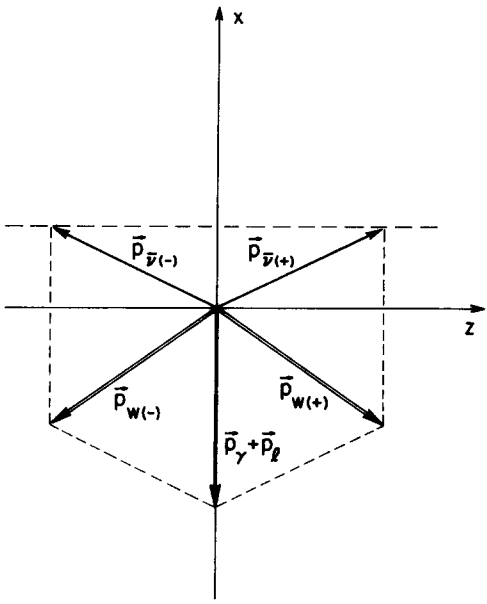

Fig. 11. Schematic view of the possible three-momentum configuration of the $\gamma\ell\bar{\nu}$ final state in the frame where $\boldsymbol{p}_\ell+\boldsymbol{p}_\gamma$ has no longitudinal component. In a typical radiative decay event, $\boldsymbol{p}_{\bar{\nu}\mathrm{T}}$ roughly balances this momentum. The two possible solutions for the neutrino three-momentum $\boldsymbol{p}_{\bar{\nu}}$ are also shown.

rapidity in the collider c.m. frame

$$y_{\bar{\nu}(\pm)} = y_{\gamma\ell} \pm \ln\left\{1+\delta+\left[\delta(2+\delta)\right]^{1/2}\right\}, \tag{2.27a}$$

where $y_{\gamma\ell}$ denotes the rapidity of the $\gamma\ell$ cluster and

$$\delta = \max\left\{m_{\mathrm{W}}^2 - m_{\mathrm{T}}^2(\gamma\ell;\bar{\nu}),0\right\}/2|\boldsymbol{p}_{\bar{\nu}\mathrm{T}}|\left[m_{\gamma\ell}^2+|\boldsymbol{p}_{\gamma\mathrm{T}}+\boldsymbol{p}_{\ell\mathrm{T}}|^2\right]^{1/2}, \tag{2.27b}$$

with the cluster transverse mass $m_{\mathrm{T}}(\gamma\ell;\bar{\nu})$ defined in eq. (2.13). The maximum symbol in eq. (2.27b) is needed because our cuts (2.24) do not eliminate completely the contribution from the "production" process (see fig. 4b) and hence $m_{\mathrm{T}}(\gamma\ell;\bar{\nu}) > m_{\mathrm{W}}$ is possible. We specify the two solutions by + and −, corresponding to the solution with $y_{\bar{\nu}} > y_{\gamma\ell}$ and $y_{\bar{\nu}} < y_{\gamma\ell}$, respectively. These two solutions coincide at the maximum value of the cluster transverse mass $m_{\mathrm{T}}(\gamma\ell;\bar{\nu}) = m_{\mathrm{W}}$.

It is now straightforward to obtain the W four-momentum for each-solution

$$p_{\mathrm{W}(\pm)} = p_\gamma + p_\ell + p_{\bar{\nu}(\pm)}. \tag{2.28}$$

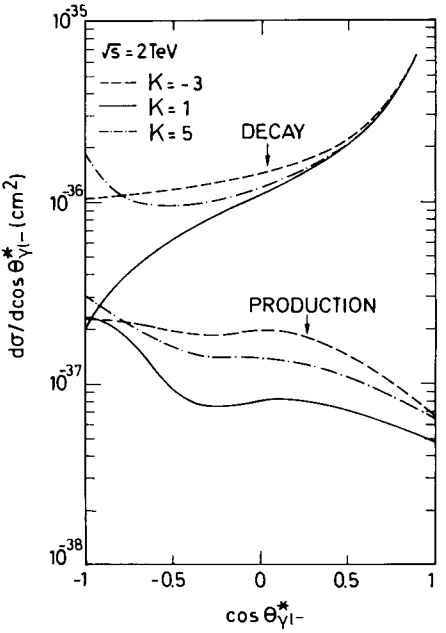

Fig. 12. $\cos\theta^*_{\gamma\ell^-}$ distribution (see eq. (2.30)) at $\sqrt{s} = 2$ TeV in the kinematical region $m_T(\gamma\ell;\bar{\nu}) < 90$ GeV. Same specifications as in fig. 7. The production process contribution for $\kappa = 1$ is the only "background" contaminating the decay contribution substantially, especially in the region of the angular zero $\cos\theta^*_{\gamma\ell^-} = -1$.

The rapidity of the W in the laboratory frame is

$$y_\pm = \ln \frac{E_{W(\pm)} + p_{Wz(\pm)}}{\left[m_W^2 + |\boldsymbol{p}_{\gamma T} + \boldsymbol{p}_{\ell T} + \boldsymbol{p}_{\bar{\nu} T}|^2\right]^{1/2}} . \tag{2.29}$$

The opening angle between the photon and the charged lepton in the W rest frame can then be expressed as

$$\cos\theta^*_{\gamma\ell\pm} = \frac{\sinh(y_\gamma - y_\pm)\sinh(y_\ell - y_\pm) + \cos\phi_{\gamma\ell}}{\cosh(y_\gamma - y_\pm)\cosh(y_\ell - y_\pm)} . \tag{2.30}$$

In fig. 12 the $\cos\theta^*_{\gamma\ell^-}$ distribution is plotted for the process $p\bar{p} \to W^- X$; $W^- \to \gamma\ell^-\bar{\nu}_\ell$ at $\sqrt{s} = 2$ TeV, with the final state cuts (2.24). The sensitivity of the distribution to κ is clearly seen. For the gauge theory case ($\kappa = 1$) there is a dip at $\cos\theta^*_{\gamma\ell^-} = -1$ which is a remnant of the zero. The shape of the distribution for non-gauge theory cases ($\kappa = -3, 5$) shows a clear difference, especially in the negative $\cos\theta^*_{\gamma\ell^-}$ region.

In low statistics experiments, it would be nice to study an integrated quantity. We define the ratio of the events with negative $\cos\theta^*_{\gamma\ell^-}$ as

$$R = \frac{N(-1 \leqslant \cos\theta^*_{\gamma\ell^-} < 0)}{N(-1 \leqslant \cos\theta^*_{\gamma\ell^-} < 0.9)}, \tag{2.31}$$

where N denotes the number of events in a specified region. We obtain from fig. 12, after summing decay and production contributions, a prediction for an arbitrary κ-value by using the formula eq. (2.23):

$$R(\sqrt{s} = 2\ \text{TeV}) = 0.264\frac{1 + 0.015(1-\kappa) + 0.049(1-\kappa)^2}{1 + 0.011(1-\kappa) + 0.016(1-\kappa)^2}. \tag{2.32}$$

The numerical uncertainties in the coefficients of eq. (2.32) are less than 5%. The ratio R is 26% for $\kappa = 1$, 38% for $\kappa = 5$ and $\kappa = -3$, at $\sqrt{s} = 2$ TeV. The ratio R is rather insensitive to $\sqrt{s}$ below Tevatron energies, since the $\sqrt{s}$ dependence enters mainly through the relative importance of the production process contribution which is small at lower energies. At the CERN $p\bar{p}$ collider energies, we find

$$R(\sqrt{s} = 540\ \text{GeV}) = 0.238\frac{1 + 0.016(1-\kappa) + 0.053(1-\kappa)^2}{1 + 0.011(1-\kappa) + 0.016(1-\kappa)^2}. \tag{2.33}$$

No significant deviation from the above values is expected at $\sqrt{s} = 630$ GeV.

Unlike in the case of $\cos\theta^*_+$ and $\cos\theta^*_-$ distributions studied in the previous subsection, we find no significant difference between $\cos\theta^*_{\gamma\ell^-}$ and $\cos\theta^*_{\gamma\ell^+}$ distributions. This can be understood since the bulk of the events have large cluster transverse mass (see fig. 4b) for which the difference between these two solutions is small (see eq. (2.27b)).

3. Effects of finite W-width and higher order QCD corrections

Up to now our presentation relied heavily on the zero width approximation for the W-boson on one hand and on lowest order QCD predictions on the other hand. In this section we discuss the effect of finite width in a quantitative way whereas only qualitative statements will be made for higher order QCD corrections, mainly focusing on the effects of non-zero transverse momentum of the W or the Wγ system.

3.1. FINITE W-WIDTH EFFECTS

Rigorously speaking, the finite width of the W-boson does not allow one to divide the process

$$d + \bar{u} \to \ell^- + \gamma + \bar{\nu}_\ell \tag{3.1}$$

into the two processes which we called "production" (2.3) and "decay" (2.4). Indeed, interference appears between the "production" and "decay" amplitudes (see the appendix for details). Since the "production" amplitude has an angular zero at $\cos\theta^*_{d\gamma} = \frac{1}{3}$ and the "decay" amplitude has a zero at $\cos\theta^*_{\gamma\ell} = -1$, it is clear that the whole contribution should vanish when both conditions

$$\cos\theta^*_{d\gamma} = \tfrac{1}{3}, \tag{3.2a}$$

$$\cos\theta^*_{\gamma\ell} = -1, \tag{3.2b}$$

are satisfied. (Note that $\theta^*_{d\gamma}$ is defined in the Wγ c.m. frame whereas $\theta^*_{\gamma\ell}$ is defined in the W rest frame.) In fact, these two conditions follow from the generalized null-radiation zone theorem [8] applied directly to the process (3.1).

Fortunately, the interference term vanishes for $\kappa = 1$ when either one of the two conditions in eq. (3.2) is satisfied. It should also be small in the dip regions and hence we do not expect large corrections from the interference. We confirmed this expectation by repeating all the numerical computations with the exact finite width formula given in the appendix. Apart from trivial kinematical effects, e.g. the smoothing of the jacobian peak in the cluster transverse mass distribution (see fig. 4b), we found no significant deviation from our zero-width results presented so far. Especially, both the $\cos\theta^*_{\pm}$ and $\cos\theta^*_{\gamma\ell_-}$ distributions agree with the zero-width results presented in fig. 6b and fig. 12, respectively, within the numerical errors of our Monte Carlo calculation.

3.2. HIGHER ORDER QCD CORRECTIONS

The problem of higher order QCD corrections is far more difficult to study quantitatively; only an explicit next-to-leading order calculation will actually tell us the significance of the corrections*. However, we shall in the following give a necessary modification of the "production" variable $\cos\theta^*_{\pm}$ in the presence of the transverse motion of the Wγ system and also give a plausible argument for the smallness of the radiative corrections to the $\cos\theta^*_{\gamma\ell_-}$ distribution in the "decay" process.

The most important QCD effect that we can anticipate without actual calculation is the non-zero transverse momentum of the Wγ system. Indeed, single and multiple gluon radiation [23] is expected to give the Wγ system a transverse momentum of about 10 GeV, which is comparable in magnitude to our transverse momentum cuts (2.12). Unless we take the transverse motion of the Wγ system into account properly, it seems clear that the dip structure would be smeared away. It is at least necessary to define the scattering angle in the Wγ c.m. frame to avoid large kinematical smearing. Indeed, the successful confrontation [24] of the dijet angular

* For first attempts toward the calculation of the higher order QCD corrections, see ref. [22].

distribution at the CERN $p\bar{p}$ collider with the lowest-order QCD prediction [25] was achieved in the dijet c.m. frame, in particular, the Collins-Soper (CS) frame [26]. The CS frame is particularly convenient, and probably gives optimal cancellation among corrections, due to its symmetric treatment of the colliding beams.

Encouraged by the success of dijet studies [24], we propose a possible modification of the $\cos\theta^*_\pm$ variable (2.18) in the presence of the non-zero transverse motion of the Wγ system:

$$\cos\tilde{\theta}^*_\pm = (p_{\gamma T}/\hat{p}_\pm)\sinh(y_\gamma - y_\pm), \tag{3.3a}$$

where $p_{\gamma T}$ and y_γ are the photon transverse momentum and rapidity, respectively, $y_\pm$ is defined in (2.17), and

$$\hat{p}_\pm = (\hat{s}_\pm - m_W^2)/2\sqrt{\hat{s}_\pm}, \tag{3.3b}$$

with

$$\hat{s}_\pm = (p_{W\pm} + p_\gamma)^2 = m_W^2 + m_{\gamma\ell}^2 + 2p_{\gamma T}p_{\bar{\nu}T}\left[\cosh(y_\gamma - y_{\bar{\nu}\pm}) - \cos\phi_{\gamma\bar{\nu}}\right]. \tag{3.3c}$$

Either $\tilde{\theta}^*_+$ or $\tilde{\theta}^*_-$ agrees in the zero W-width limit with the γ polar angle in the CS frame of the Wγ system. This new variable reduces to our old one (2.18) in the zero transverse momentum limit of the Wγ system. Hence the $\cos\theta^*_\pm$ distributions shown in fig. 6 are also the $\cos\tilde{\theta}^*_\pm$ distributions in the lowest order. Higher order corrections can, however, be significantly different between the two distributions. We examined the effect of purely kinematical smearings by giving both colliding partons the gaussian transverse momentum distributions with $\langle p_T\rangle = 7$ GeV; the $\cos\tilde{\theta}^*_-$ distribution received small corrections while the dip in the $\cos\theta^*_-$ distribution almost disappeared.

It is therefore important to look for a "good" variable whose distribution receives small corrections in the future next-to-leading order studies. Guided by the successful dijet studies, we propose the variable $\cos\tilde{\theta}^*_-$ as a candidate. Since our interest is in the dip structure of distributions, it is not clear at present whether such a "good" variable exists or not.

On the other hand, the situation is much better in the W radiative decay studies, where we expect small corrections in the $\cos\theta^*_{\gamma\ell^-}$ distributions. First of all, the variable $\cos\theta^*_{\gamma\ell^-}$ (2.30) refers to the W-rest frame variable even in the presence of a W transverse motion. Hence gluon radiation can affect the distribution only through the W-polarization. On one hand this cannot influence the distribution near the zero at $\cos\theta^*_{\gamma\ell} = -1$ because every polarization amplitude has a common zero at that point [19]. On the other hand, the whole distribution is rather insensitive to W polarizations as can be seen from comparing the distribution from an unpolarized W (fig. 9) and that of a longitudinally polarized W (fig. 12). The main uncertainty thus enters through the extra contribution from the Wγ production process (see fig. 12), whose magnitude is small anyway in most of the $\cos\theta^*_{\gamma\ell^-}$ range.

4. Backgrounds

In this section we study background contributions to the production process (2.3) as well as to the decay process (2.4). A large p_T isolated charged lepton with large $\not{p}_T$ can come either from W or heavy quark pair production. Pair production of a heavy quark (top [27,28] or even heavier quarks [29]), however, typically ends up with multi-jet events and is unlikely to fake our signal. A significant background is expected from the process

$$\begin{array}{l} p + \bar{p} \to W^- + \text{jet} + \text{anything} \\ \qquad\quad \big\lfloor \to \ell + \bar{\nu}\,, \end{array} \tag{4.1}$$

where a high p_T jet resembles a high p_T photon through γ/π^0 misidentification. Since the W-jet production cross section is roughly a factor of α_s/α larger than the $W\gamma$ production cross section, and since the κ dependence of the distribution is more pronounced in the dip region, the background contribution severely restricts the sensitivity of our measurement of κ. On the other hand, the W radiative decay experiment is found to be rather free from large backgrounds. The main restrictive factor here is then statistics since the κ-dependence in this process is milder than in the case of W production.

4.1. BACKGROUNDS FOR $p\bar{p} \to W^- \gamma X$; $W^- \to \ell\bar{\nu}_\ell$

In this subsection we study backgrounds for the production process (2.3). A severe background is expected from the W-jet production process (4.1) where a high p_T jet fakes a single high p_T photon. The lowest order subprocesses which contribute to W^- jet production are

$$d + \bar{u} \to W^- + \text{gluon}\,, \tag{4.2a}$$

$$d + \text{gluon} \to W^- + u\,, \tag{4.2b}$$

$$\bar{u} + \text{gluon} \to W^- + \bar{d}\,. \tag{4.2c}$$

The production cross section for these subprocesses including the subsequent decay of $W \to \ell\bar{\nu}$ can be obtained from the appendix; only color factors and coupling constants have to be changed. (See also the published literature [10].) We use the same parton distribution [15,16] as in sect. 2 and for the QCD running coupling constant we take

$$\alpha_s(\hat{s}) = 12\pi/(33 - 2n)\ln(\hat{s}/\Lambda_n^2)\,, \tag{4.3}$$

where n is the number of the active flavors and $\hat{s}$ the squared mass of the colliding

parton system. The flavor number is increased by one at each threshold, $\sqrt{\hat{s}} = 2m_n$; the continuity of α_s is maintained by choice of the Λ_n. We choose $\Lambda_4 = 0.3$ GeV, $m_b = 5$ GeV, and $m_t = 35$ GeV for definiteness.

After imposing the cuts (2.12) and (2.14) by replacing the photon by the jet, we find at $\sqrt{s} = 2$ TeV a cross section of about 0.16 nb for the $W^- \to e\bar{\nu}_e$ channel. The background contribution is then obtained by multiplying this cross section by the probability $P_{\gamma/j}$ that a jet is misidentified as a single isolated photon. A precise value for $P_{\gamma/j}$ depends on details of the jet structure and of the detector. For the cut $p_{\gamma T} > 10$ GeV, a BNL study group reported [20] values between $\frac{1}{230}$ and $\frac{1}{500}$, depending on the resolution of the γ shower detector. In the following, we choose a value

$$P_{\gamma/j} = \tfrac{1}{200} \tag{4.4}$$

for the background estimate. We choose this rather pessimistic value because of the uncertainties in our computation of the signal-to-background ratio: The γ/jet misidentification probability should be different for gluon and quark jets and hence between $p\bar{p}$ reactions where the "annihilation" subprocess (4.2a) dominates (at $\sqrt{s} = 2$ TeV about 70% of the total W-jet events come from (4.2a)) and pp reactions where the "Compton" subprocess (4.2b) and (4.2c) are more important. Furthermore, the QCD higher order effects including multigluon emission can affect somewhat differently the signal and background contributions. In actual experiments, a reliable estimate for the probability $P_{\gamma/j}$ is essential to estimate the background and hence to determine the value of κ. It is therefore very important to determine $P_{\gamma/j}$ in prompt photon experiments at hadron colliders.

In fig. 13 we plotted again our predictions for the $\cos\theta^*$ distributions of the signal events for several values of κ in $p\bar{p}$ collisions at $\sqrt{s} = 2$ TeV. In the same figures we show by the dashed line the background W-jet contribution multiplied by the factor $P_{\gamma/j} = \frac{1}{200}$ (eg. (4.4)): the integrated cross section for the $\kappa = 1$ signal and the background are roughly the same, about 3 pb after summing up $e^{\pm}$ and $\mu^{\pm}$ modes. Without including the QCD motivated K-factor we expect 300 events for both signal and backgrounds with a nominal integrated luminosity of 10^{38} cm^{-2}. The shape of the distributions are, however, very different for small $|\kappa - 1|$. At $|\kappa - 1| = 5$, the shape of the signal and the background become more or less the same. In order to determine the κ-value from the observed distribution, which is the sum of the signal and background contributions, we need to estimate both the magnitude and the shape of the backgrounds. The shape of the background distribution can be determined rather well by the jet trigger experiments, while its magnitude is essentially determined by the factor $P_{\gamma/j}$. It seems to be difficult to obtain a bound stronger than $|\kappa - 1| < 2$ because the background dominates over the signal for $|\kappa - 1| < 2$ in the dip region where the κ-dependence is strongest.

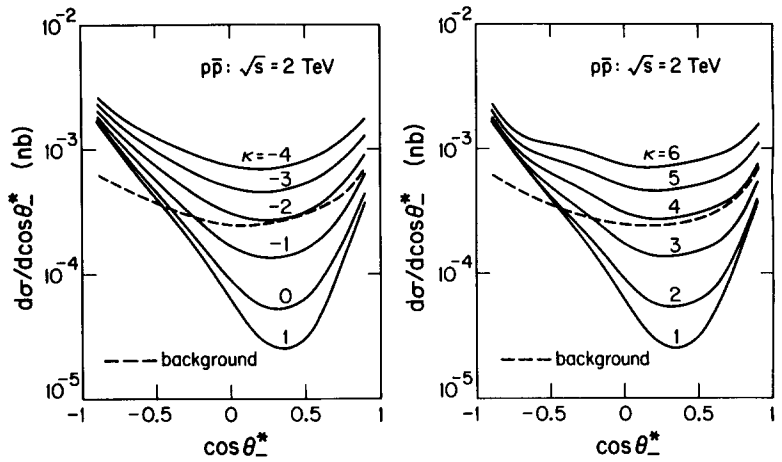

Fig. 13. $\cos\theta^*_-$ distribution for the production process $p\bar{p} \to W^-\gamma X$; $W^- \to \ell^-\bar{\nu}_\ell$ at $\sqrt{s} = 2$ TeV for different values of κ. The cuts are specified by eqs. (2.12) and (2.14). The dashed lines denote the estimated background from $p\bar{p} \to W(\text{"}\gamma\text{"})X$ where "γ" represents a jet that may fake photons.

4.2. BACKGROUNDS FOR $p\bar{p} \to W^- X$; $W^- \to \gamma\ell^-\bar{\nu}_\ell$

As studied in sects. 2 and 3, there are two advantages and one disadvantage in measuring κ in W production followed by its radiative decay, $W^- \to \gamma\ell^-\bar{\nu}_\ell$. The two advantages are the relatively larger cross section and the insensitivity of the analysis on the transverse motion of the W. The disadvantage is the fact that the κ-dependence of the signature is not as spectacular as that for the $W\gamma$ production case. In the following we will find another advantage in studying W radiative decay, the large signal-to-background ratio.

In terms of observable momenta, the W radiative decay process can be specified by the events satisfying the following cuts (see (2.24)):

$$p_{\gamma T},\ p_{\ell T} > 10\ \text{GeV}; \qquad |y_\gamma|,\ |y_\ell| < 3,$$

$$30\ \text{GeV} < m_T(\gamma\ell;\ \text{missing}) < 90\ \text{GeV},$$

$$\cos\theta_{\gamma\ell} < 0.95. \tag{4.5}$$

A significant background can again come from W-jet production processes (4.2) where the jet is misidentified as a single photon. We find that roughly one-third of the jet-plus-$\ell\bar{\nu}$ events have a cluster transverse mass $m_T(\ell\,\text{jet};\bar{\nu})$ smaller than 90 GeV. Furthermore, the contribution from W-jet production followed by the decay $W^- \to \tau\ \bar{\nu}_\tau$ is non-negligible since a substantial portion of the events with a subsequent $\tau \to e$ or μ decay survives the cuts (4.5) when we replace a photon by a jet. In this evaluation we use the branching ratio $B(\tau \to e) = 0.17$ and the purely

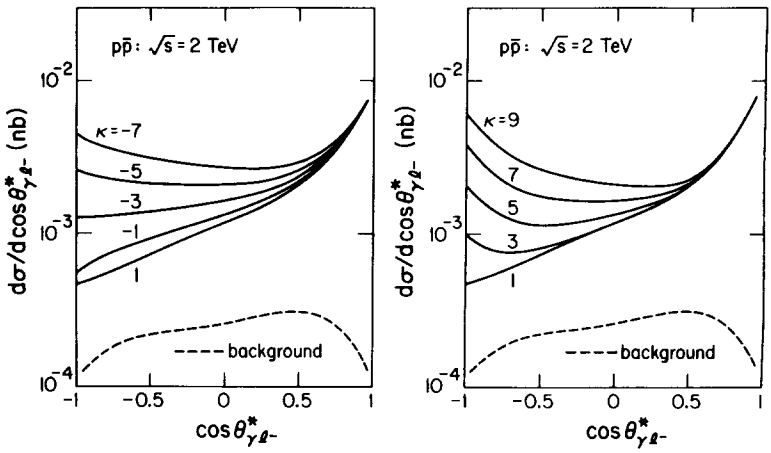

Fig. 14. $\cos\theta^*_{\gamma\ell^-}$ distribution at $\sqrt{s} = 2$ TeV for different values of κ in the kinematical region $m_T(\gamma\ell^-; \bar{\nu}) < 90$ GeV. The contributions from decay and production processes which were shown separately in fig. 12 are added together. The cuts are specified by eq. (2.24). The dashed lines denote the estimated background from $p\bar{p} \to W^-$"γ"X, where "γ" represents a jet that may fake photons.

left-handed $\tau \to e$ decay distribution calculated in the $V-A$ theory. The missing transverse momentum ($\not{p}_T$) in this case is the vector sum of all the neutrino transverse momenta. We find that the cascade $W \to \tau \to e$ decay contribution to the background is about 20% of the direct $W^- \to e\bar{\nu}$ contribution. The background shown below is the sum of these two contributions.

In fig. 14 we show our predictions for the $\cos\theta^*_{\gamma\ell^-}$ distributions of the radiative W decay signal events for several values of κ in $p\bar{p}$-collisions at $\sqrt{s} = 2$ TeV. The dashed line represents the background contribution, again multiplied by the γ/jet misidentification probability $P_{\gamma/j} = \frac{1}{200}$ (see eq. (4.4)). The signal curves are just the sum of the pure $W \to e\bar{\nu}\gamma$ (decay) contribution and the $W\gamma$ production contribution shown separately in fig. 12, which satisfy the final state cuts (4.5) or (2.24). Contributions from the cascade processes $W \to \tau\bar{\nu}\gamma$; $\tau \to e$ and $W\gamma$; $W \to \tau\bar{\nu}$; $\tau \to e$ are both found to be negligible. From this figure we find that the estimated background is always smaller than the signal cross section, even in the dip region around $\cos\theta^*_{\gamma\ell^-} = -1$ for the $\kappa = 1$ case. The shape of the distribution is also very different between the signal and the background. Hence, an error in the estimate of the magnitude of the background by as much as 100% (i.e. in the γ/jet misidentification probability $P_{\gamma/j}$) does not severely restrict the measurement of κ.

5. Summary and discussion

In this paper we examined the feasibility to measure the $WW\gamma$ triple gauge coupling at proton-antiproton colliders through the process $p\bar{p} \to \gamma\ell^-\bar{\nu}_\ell X$. To quan-

tify this measurement, we allow arbitrary real value for the anomalous magnetic moment [5] κ of the W-boson. In any gauge theory of the electroweak interaction, the κ value should be unity up to $O(\alpha)$ corrections. Hence any measurement of κ different from unity signals the failure of gauge theories in the weak interaction.

In the zero-width approximation for the W propagator the $\ell\bar{\nu}\gamma$ final state can originate either from the "production" process $p\bar{p} \to W^-\gamma X$ with the subsequent $W^- \to \ell^-\bar{\nu}_\ell$ decay or from the "decay" process $p\bar{p} \to W^- X$ with the W^- decaying radiatively into $\ell\bar{\nu}\gamma$. We found that these two processes can be kept apart rather effectively by imposing a cut in the cluster transverse mass variable, $m_T(\ell\gamma; \bar{\nu})$.

The cross sections of the subprocess $d\bar{u} \to W^-\gamma$ and $W^- \to \gamma\ell\bar{\nu}$ vanish at specific kinematical configurations [7, 8], $\cos\theta^*_{d\gamma} = \frac{1}{3}$ in the $W\gamma$ c.m. frame and $\cos\theta^*_{\gamma\ell} = -1$ in the W rest frame, if $\kappa = 1$, the gauge theory value. A unique reconstruction of these angular variables from the observable momenta, $\boldsymbol{p}_\gamma$, $\boldsymbol{p}_\ell$, and the missing p_T vector is not possible, allowing for the two-fold ambiguity in the W-longitudinal momentum in the zero width limit. We find, however, that κ-sensitive distributions can still be obtained in terms of the variables $\cos\theta^*_-$ (2.18) and $\cos\theta^*_{\gamma\ell_-}$ (2.30), which are defined in terms only of observable momenta in such a way that in most of the cases they coincide with either $\cos\theta^*_{d\gamma}$ or $\cos\theta^*_{\gamma\ell}$, respectively, in the zero W-width limit. The κ-sensitivity of the $\cos\theta^*_-$ distribution near the dip at $\cos\theta^*_- = \frac{1}{3}$ is found to be spectacular, giving a cross section for $|\kappa - 1| = 2$ which is an order of magnitude higher than the one corresponding to $\kappa = 1$, the gauge theory value. The κ-sensitivity of the $\cos\theta^*_{\gamma\ell_-}$ distribution is found to be moderate due to the fact that the W-radiative decay distribution vanishes at $\kappa = 1$ only linearly (and not quadratically, as in $W\gamma$ production) when the angular zero point is approached.

The effects of the finite W width on both distributions are found to be negligible. A more serious problem is to estimate higher order QCD corrections. Especially large corrections are expected for the $\cos\theta^*_-$ distribution from the transverse motion of the $W\gamma$ system. We argued that at least a modification of the variable, e.g. $\cos\tilde{\theta}^*_-$ as defined in eq. (3.3), is necessary to make the correction smaller. Whether such a modification of the variable is sufficient or not, we will learn only after serious next-to-leading order studies. The situation in the case of $\cos\theta^*_{\gamma\ell_-}$ distribution is much better, for which we presented a plausible argument for the smallness of the QCD radiative corrections. This is mainly due to the fact that the quantity $\cos\theta^*_{\gamma\ell}$ refers to the variable in the W rest frame independent of the W transverse motion.

Backgrounds due to the W + jet production where the jet is misidentified as a single isolated photon were also studied. We estimated the effects of such contributions by assuming the γ/jet misidentification probability $P_{\gamma/j}$ to be $\frac{1}{200}$. The background is found to affect the measurement of κ seriously in the production signal ($\cos\theta^*_-$ distribution) while it is expected to be less dangerous in the radiative decay signal ($\cos\theta^*_{\gamma\ell_-}$ distribution).

On the experimental side the most serious problem is the photon identification at relatively small p_T (> 10 GeV). It is also important to reduce the error of the

missing transverse momentum $\not{p}_T$ in order for the $m_T(\ell\gamma; \bar{\nu})$ cut (to distinguish production from decay) to be fully effective. Once those conditions, as well as the requirement for high luminosity, are met, we find it feasible to measure the WWγ coupling at $p\bar{p}$ colliders, especially in the W radiative decay signals. Adding up $e^{\pm}$ and $\mu^{\pm}$ contributions, the expected event rates for $\kappa = 1$ at the Fermilab collider ($\sqrt{s} = 2$ TeV) are, after applying all the final state cuts (2.12), (2.14) and (2.24), respectively,

30 events for "production" signal,

135 events for "decay" signal,

with a nominal integrated luminosity of 10^{37} cm^{-2}. Event rates one order of magnitude smaller are expected at the CERN collider. High luminosity is clearly the basic requirement for the measurements.

We conclude by listing advantages and disadvantages of the two signal processes in measuring κ. The Wγ production signal gives a spectacular κ dependence but has a smaller cross section, a larger background contamination and is most likely to be rather sensitive to QCD higher-order corrections. The W radiative decay signal gives a moderate κ-dependence while it has a relatively larger cross section, a small background contamination and is insensitive to higher-order QCD corrections.

Part of the results had been reported at 4th Topical Workshop on Proton Antiproton Collider Physics [30].

The authors wish to thank V. Barger, M. Ebel, C. Goebel, F. Halzen, K. Hikasa, S. Jacobs, A. Kronfeld and Y. Okamoto for useful discussions. The work of J.C. is partially supported by CAICYT and Comisión de Intercambio Cultural. The work of F.H. is supported by the Swiss National Science Foundation and partially by the Max Geldner Stiftung. This work was started when all the authors were at University of Wisconsin-Madison, where it was supported in part by the University of Wisconsin Research Committee with funds granted by the Wisconsin Alumni Research Foundation, and in part by the Department of Energy under contract DE-AC02-76ER00881.

Appendix

In this appendix we present the complete partonic cross section for the process $d\bar{u} \to \gamma\ell\bar{\nu}$; all fermion masses will be neglected. The Feynman diagrams of this process are shown in fig. 1.

Using the shorthand notation

$$p = p_d, \qquad \bar{p} = p_{\bar{u}}, \qquad k = p_\gamma, \qquad \ell = p_\ell, \qquad \bar{\ell} = p_{\bar{\nu}}, \qquad P = p + \bar{p} \quad \text{(A.1)}$$

for the four-momenta of the particles involved, the amplitude can be written as

$$\mathcal{M} = \frac{(4\pi\alpha)^{3/2}}{2\sin^2\theta_W}\left\{\bar{v}(\bar{p})P_{\rho\alpha}u(p)\frac{\varepsilon^\alpha(k)^* J_\ell^\rho}{(P-k)^2 - m_W^2 + im_W\Gamma_W}\right.$$

$$\left. + \bar{u}(\ell)D_{\rho\alpha}v(\bar{\ell})\frac{\varepsilon^\alpha(k)^* J_p^\rho}{P^2 - m_W^2 + im_W\Gamma_W}\right\}. \qquad \text{(A.2)}$$

α is the fine structure constant, θ_W the Weinberg angle and $m_W(\Gamma_W)$ the mass (width) of the W-boson. The tensors $P_{\rho\alpha}$ and $D_{\rho\alpha}$ are given by

$$P_{\rho\alpha} = \left\{F_c\left[\gamma_\rho\frac{\not{k}-\not{p}}{k\cdot p}\gamma_\alpha + \gamma_\alpha\frac{\not{\bar{p}}-\not{k}}{\bar{p}\cdot k}\gamma_\rho\right] + (1-\kappa)\frac{\not{k}g_{\rho\alpha} - k_\rho\gamma_\alpha}{P\cdot k}\right\}\frac{1-\gamma_5}{4}, \qquad \text{(A.3a)}$$

$$D_{\rho\alpha} = \left\{\bar{F}_c\left[\gamma_\rho\frac{\not{k}+\not{\bar{\ell}}}{k\cdot\bar{\ell}}\gamma_\alpha - \gamma_\alpha\frac{\not{k}+\not{\ell}}{k\cdot\ell}\gamma_\rho\right] + (1-\kappa)\frac{\not{k}g_{\rho\alpha} - k_\rho\gamma_\alpha}{P\cdot k}\right\}\frac{1-\gamma_5}{4}, \qquad \text{(A.3b)}$$

with two charge-dependent factors

$$F_c = \frac{Q_u\, p\cdot k + Q_d\,\bar{p}\cdot k}{P\cdot k}, \qquad \bar{F}_c = \frac{k\cdot\bar{\ell}}{P\cdot k}. \qquad \text{(A.4)}$$

The tensors $P_{\rho\alpha}$ and $D_{\rho\alpha}$ satisfy the current conservation conditions

$$k^\alpha P_{\rho\alpha} = k^\alpha D_{\rho\alpha} = 0.$$

In addition we defined the lepton and quark currents,

$$J_\ell^\rho = \bar{u}(\ell)\gamma^\rho\frac{1-\gamma_5}{2}v(\bar{\ell}), \qquad J_p^\rho = \bar{v}(\bar{p})\gamma^\rho\frac{1-\gamma_5}{2}u(p). \qquad \text{(A.5)}$$

In order to write the amplitude $\mathcal{M}$ in the form (A.2) we made use of the partial fraction decomposition of the propagator product

$$\frac{1}{(P-k)^2 - m_W^2 + im_W\Gamma_W}\,\frac{1}{P^2 - m_W^2 + im_W\Gamma_W}$$

$$= \frac{1}{2P\cdot k}\left[\frac{1}{(P-k)^2 - m_W^2 + im_W\Gamma_W} - \frac{1}{P^2 - m_W^2 + im_W\Gamma_W}\right] \qquad \text{(A.6)}$$

and of the factorization property, as discussed in sects. 1 and 2. In this decomposi-

tion of the amplitude, which is called the radiation decomposition by Brodsky and Brown [8], it is evident that the amplitude has a zero at

$$F_c = \bar{F}_c = 0$$

in the gauge theory case, $\kappa = 1$.

The squared matrix element, summed (averaged) over final (initial) spin and colors, reads

$$\overline{\sum}|\mathcal{M}|^2 = \frac{(4\pi\alpha)^3}{4\sin^4\theta_W}\left\{\frac{1}{\left[(P-k)^2 - m_W^2\right]^2 + m_W^2\Gamma_W^2}\right.$$
$$\times\left[\mathbb{P} + \frac{A\left[(P-k)^2 - m_W^2\right] + Bm_W\Gamma_W}{P\cdot k}\right]$$
$$\left. + \frac{1}{\left[P^2 - m_W^2\right]^2 + m_W^2\Gamma_W^2}\left[\mathbb{D} - \frac{A\left[P^2 - m_W^2\right] + Bm_W\Gamma_W}{P\cdot k}\right]\right\}. \quad \text{(A.7)}$$

Here $\mathbb{P}$ denotes the contribution which we labeled "production" and its explicit form is given by:

$$\mathbb{P} = \sum_{i=1}^{6} \alpha_i H_i, \quad \text{(A.8a)}$$

where

$$\alpha_1 = 4\ell\cdot\bar{\ell},$$
$$\alpha_2 = 2(p\cdot\ell)(p\cdot\bar{\ell})/(\ell\cdot\bar{\ell}),$$
$$\alpha_3 = 2(\bar{p}\cdot\ell)(\bar{p}\cdot\bar{\ell})/(\ell\cdot\bar{\ell}),$$
$$\alpha_4 = 4(p\cdot\bar{\ell})(\bar{p}\cdot\ell)/(\ell\cdot\bar{\ell}) - 2p\cdot\bar{p},$$
$$\alpha_5 = 2p\cdot(\bar{\ell}-\ell),$$
$$\alpha_6 = 2\bar{p}\cdot(\bar{\ell}-\ell), \quad \text{(A.8b)}$$

and

$$H_1 = \frac{1}{2N}\left\{ F_c^2 \frac{\hat{t}^2+\hat{u}^2+4\ell\cdot\bar{\ell}\hat{s}}{\hat{t}\hat{u}} + F_c(1-\kappa)\frac{\hat{t}-\hat{u}}{\hat{t}+\hat{u}} + (1-\kappa)^2\frac{\hat{t}\hat{u}}{2(\hat{t}+\hat{u})^2}\right\},$$

$$H_2 = -\frac{2\ell\cdot\bar{\ell}}{N}\left\{ F_c^2 \frac{4\ell\cdot\bar{\ell}}{\hat{t}\hat{u}} + F_c(1-\kappa)\frac{2\ell\cdot\bar{\ell}+\hat{t}}{\hat{t}(\hat{t}+\hat{u})} + (1-\kappa)^2\frac{\hat{u}}{2(\hat{t}+\hat{u})^2}\right\},$$

$$H_3 = -\frac{2\ell\cdot\bar{\ell}}{N}\left\{ F_c^2 \frac{4\ell\cdot\bar{\ell}}{\hat{t}\hat{u}} - F_c(1-\kappa)\frac{2\ell\cdot\bar{\ell}+\hat{u}}{\hat{u}(\hat{t}+\hat{u})} + (1-\kappa)^2\frac{\hat{t}}{2(\hat{t}+\hat{u})^2}\right\},$$

$$H_4 = \frac{\ell\cdot\bar{\ell}}{N}\left\{ F_c(1-\kappa)\frac{\hat{s}(\hat{t}-\hat{u})}{\hat{t}\hat{u}(\hat{t}+\hat{u})} - (1-\kappa)^2\frac{1}{2(\hat{t}+\hat{u})}\right\},$$

$$H_5 = \frac{\ell\cdot\bar{\ell}}{N}\left\{ F_c^2 \frac{4\ell\cdot\bar{\ell}-2\hat{u}}{\hat{t}\hat{u}} + F_c(1-\kappa)\frac{\hat{s}+2\hat{t}}{\hat{t}(\hat{t}+\hat{u})} + (1-\kappa)^2\frac{\hat{u}}{2(\hat{t}+\hat{u})^2}\right\},$$

$$H_6 = \frac{\ell\cdot\bar{\ell}}{N}\left\{ F_c^2 \frac{-4\ell\cdot\bar{\ell}+2\hat{t}}{\hat{t}\hat{u}} + F_c(1-\kappa)\frac{\hat{s}+2\hat{u}}{\hat{u}(\hat{t}+\hat{u})} - (1-\kappa)^2\frac{\hat{t}}{2(\hat{t}+\hat{u})^2}\right\}. \quad \text{(A.8c)}$$

In these expressions we introduced the usual partonic Mandelstam variables

$$\hat{s} = (p+\bar{p})^2,$$

$$\hat{t} = (k-p)^2,$$

$$\hat{u} = (k-\bar{p})^2, \quad \text{(A.9)}$$

and $N = 3$ for QCD. Similarly, the term $\mathbb{D}$ in (A.7) corresponds to the "decay" contribution and its explicit form can be obtained from $\mathbb{P}$ by the following substitutions:

$$\mathbb{D} = \mathbb{P}(p \to -\bar{\ell}, \bar{p} \to -\ell, k \to k, \ell \to -\bar{p}, \bar{\ell} \to -p, Q_u \to 1, Q_d \to 0). \quad \text{(A.10)}$$

The quantities A and B in eq. (A.7) refer to the real and imaginary part of the interference term, respectively. Their evaluation is simplified by the use of identities given by Sirlin [31]. One finds for the real part

$$A = 8F_c\bar{F}_c A_1 + 4F_c(1-\kappa)A_2 + 4\bar{F}_c(1-\kappa)A_3 + 4(1-\kappa)^2 A_4, \quad \text{(A.11a)}$$

with

$$A_1 = -\frac{\bar{p}\cdot\ell p\cdot(k+\bar{\ell})\bar{\ell}\cdot(p-k)}{p\cdot kk\cdot\bar{\ell}} - \frac{p\cdot\bar{\ell}\bar{p}\cdot(k+\ell)\ell\cdot(\bar{p}-k)}{\bar{p}\cdot kk\cdot\ell}$$

$$+\left\{\frac{1}{\bar{p}\cdot kk\cdot\bar{\ell}}\left[2\bar{p}\cdot\bar{\ell}p\cdot\bar{\ell}\bar{p}\cdot\ell+\bar{p}\cdot\ell(p\cdot k\bar{p}\cdot\bar{\ell}+\bar{p}\cdot kp\cdot\bar{\ell}-p\cdot\bar{p}k\cdot\bar{\ell})\right.\right.$$

$$-p\cdot\bar{\ell}(\bar{p}\cdot\bar{\ell}k\cdot\ell+\bar{p}\cdot\ell k\cdot\bar{\ell}-\ell\cdot\bar{\ell}\bar{p}\cdot k)]$$

$$\left.+(p\leftrightarrow-\bar{\ell},\bar{p}\leftrightarrow-\ell)\right\}, \tag{A.11b}$$

$$A_2 = \frac{1}{P\cdot k}\left\{2p\cdot\bar{\ell}k\cdot\ell-2\bar{p}\cdot\ell k\cdot\bar{\ell}+\frac{p\cdot\bar{\ell}}{p\cdot k}[p\cdot\ell\bar{p}\cdot k-p\cdot\bar{p}k\cdot\ell]\right.$$

$$\left.-\frac{\bar{p}\cdot\ell}{\bar{p}\cdot k}[\bar{p}\cdot\bar{\ell}p\cdot k-p\cdot\bar{p}k\cdot\bar{\ell}]\right\}, \tag{A.11c}$$

$$A_3 = A_2(p\leftrightarrow-\bar{\ell},\bar{p}\leftrightarrow-\ell), \tag{A.11d}$$

$$A_4 = (P\cdot k)^{-2}[p\cdot k\bar{p}\cdot\ell k\cdot\bar{\ell}+\bar{p}\cdot kp\cdot\bar{\ell}k\cdot\ell]. \tag{A.11e}$$

For the imaginary part we find

$$B = 4\varepsilon_{\alpha\beta\gamma\delta}p^{\alpha}\bar{p}^{\beta}k^{\gamma}\ell^{\delta}[2F_c\bar{F}_cB_1+F_c(1-\kappa)B_2+\bar{F}_c(1-\kappa)B_3], \tag{A.12a}$$

with $\varepsilon_{0123}=1$,

$$B_1 = -\frac{\bar{p}\cdot\ell+p\cdot\bar{\ell}}{\bar{p}\cdot kk\cdot\bar{\ell}}+\frac{\bar{p}\cdot\ell+p\cdot\bar{\ell}}{p\cdot kk\cdot\ell}, \tag{A.12b}$$

$$B_2 = \frac{1}{P\cdot k}\left\{\frac{\bar{p}\cdot\ell}{\bar{p}\cdot k}+\frac{p\cdot\bar{\ell}}{p\cdot k}\right\}, \tag{A.12c}$$

$$B_3 = B_2(p\leftrightarrow-\bar{\ell},\bar{p}\leftrightarrow-\ell). \tag{A.12d}$$

In the case of the zero width approximation there is no interference between the production and the decay process; the terms A and B can thus be dropped safely. The production process will be given by

$$\overline{\sum}|\mathcal{M}(q\bar{q}'\to W^-\gamma;W^-\to\ell\bar{\nu})|^2 = \frac{(4\pi\alpha)^3}{4\sin^4\theta_W}\frac{\pi}{m_W\Gamma_W}\mathbb{P}\delta[(P-k)^2-m_W^2] \tag{A.13}$$

and similarly for the decay process:

$$\overline{\sum}|\mathcal{M}(q\bar{q}' \to W^-; W^- \to \gamma\ell\bar{\nu})|^2 = \frac{(4\pi\alpha)^3}{4\sin^4\theta_W}\frac{\pi}{m_W\Gamma_W}\mathbb{D}\delta(P^2 - m_W^2). \quad (A.14)$$

In the case $\kappa = 1$ the sum (A.8a) can be performed to arrive at a simple expression. For the production process we find

$$\overline{\sum}|\mathcal{M}(q\bar{q}' \to W^-\gamma; W^- \to \ell\bar{\nu})|^2$$

$$= \frac{128\pi^4\alpha^2}{\sin^2\theta_W}B(W \to \ell\bar{\nu})\frac{4F_c^2\left[(\bar{p}\cdot\ell)^2 + (p\cdot\bar{\ell})^2\right]}{\hat{t}\hat{u}}\delta\left[(P-k)^2 - m_W^2\right]. \quad (A.15)$$

For the decay process we apply on eq. (A.15) the substitution rule (A.10) to get

$$\overline{\sum}|\mathcal{M}(q\bar{q}' \to W^-; W^- \to \gamma\ell\bar{\nu})|^2$$

$$= \frac{128\pi^4\alpha^2}{\sin^2\theta_W}B(W \to \ell\bar{\nu})\frac{\bar{F}_c^2\left[(\bar{p}\cdot\ell)^2 + (p\cdot\bar{\ell})^2\right]}{(k\cdot\ell)(k\cdot\bar{\ell})}\delta(P^2 - m_W^2). \quad (A.16)$$

References

[1] J. Cortés, K. Hagiwara and F. Herzog, Wisconsin preprints MAD/PH/102 (1983), MAD/PH/108 (1983), MAD/PH/164 (1984)

[2] UA1 collaboration, Phys. Lett. 122B (1983) 103, 126B (1982) 398;
UA2 collaboration, Phys. Lett. 122B (1983) 476, 129B (1983) 130

[3] S.L. Glashow, Nucl. Phys. 22 (1961) 579;
S. Weinberg, Phys. Rev. Lett. 19 (1967) 1264;
A. Salam, *in* Elementary particle theory, ed. N. Svartholm (Almquist and Wiksell, Stockholm, 1968), p. 367

[4] P.Q. Hung and J.J. Sakurai, Nucl. Phys. B143 (1978) 81;
J.D. Bjorken, Phys. Rev. D19 (1979) 335

[5] T.D. Lee and C.N. Yang, Phys. Rev. 128 (1962) 885

[6] W.A. Bardeen, R. Gastmans and B. Lautrup, Nucl. Phys. B46 (1972) 319

[7] K.O. Mikaelian, Phys. Rev. D17 (1978) 750;
R.W. Brown, D. Sahdev and K.O. Mikaelian, Phys. Rev. D20 (1979) 1164;
K.O. Mikaelian, M.A. Samuel and D. Sahdev, Phys. Rev. Lett. 43 (1979) 746;
J.D. Stroughair and C.L. Bilchak, Z. Phys. C26 (1984) 415

[8] Zhu Dongpei, Phys. Rev. D22 (1980) 2266;
C.J. Goebel, F. Halzen and J.P. Leveille, Phys. Rev. D23 (1981) 2682;
S.J. Brodsky and R.W. Brown, Phys. Rev. Lett. 49 (1982) 966;
M.A. Samuel, Phys. Rev. D27 (1983) 2724;
R.W. Brown, K.L. Kowalski and S.J. Brodsky, Phys. Rev. D28 (1983) 624

[9] V. Barger, A.D. Martin and R.J.N. Phillips, Phys. Lett. 125B (1983) 339;
E.L. Berger, D. Di Bitonto, M. Jacob and W.J. Stirling, Phys. Lett. 140B (1984) 259

[10] M. Chaichian, M. Hayashi and K. Yamagishi, Phys. Rev. D25 (1982) 130, E26 (1982) 2534
[11] S. Drell and T.M. Yan, Ann. of Phys. 66 (1971) 578
[12] H. Aronson, Phys. Rev. 186 (1969) 1434;
K.J. Kim and Y.S. Tsai, Phys. Rev. D7 (1973) 3710
[13] R. Robinettt, Phys. Rev. D28 (1983) 1185;
K. Hikasa, Phys. Lett. 128B (1983) 253
[14] H.D. Politzer, Nucl. Phys. B129 (1977) 301;
D. Amati, R. Petronzio and G. Veneziano, Nucl. Phys. B140 (1978) 54;
R.K. Ellis, H. Georgi, M. Machacek, H.D. Politzer and G.G. Ross, Nucl. Pys. B152 (1979) 285;
A.H. Mueller, Phys. Rev. D18 (1978) 3705
[15] A.J. Buras and K.J.F. Gaemers, Nucl. Phys. B132 (1978) 249
[16] J.F. Owens and E. Reya, Phys. Rev. D17 (1978) 3003
[17] C. Quigg, Rev. Mod. Phys. 49 (1977) 297
[18] E.L. Berger, *in* Proc. Workshop on Drell-Yan-processes, 1982
[19] M. Hellmund and G. Ranft, Z. Phys. C12 (1982) 333;
J. Cortés, K. Hagiwara and F. Herzog, Phys. Rev. D28 (1983) 2311
[20] S.A. Kahn, I.J. Killian, M.J. Murtagh and F.E. Paige, BNL informal report 3/83 (1983)
[21] T.R. Grose and K.O. Mikaelian, Phys. Rev. D23 (1981) 123
[22] N.M. Monyonko and J.H. Reid, *in* Proc. Workshop on Nonperturbative QCD, ed. K.A. Milton and M.A. Samuel, Oklahoma State Univ., March 1983;
M.L. Laursen and M.A. Samuel, Oklahoma State Univ. preprint No. 137 (1982);
A. Sen, Phys. Rev. D28 (1983) 650;
M.L. Laursen, M.A. Samuel, A. Sen and G. Tupper, Nucl. Phys. B226 (1983) 429;
G. Tupper, Phys. Lett. 156B (1985) 406
[23] G. Altarelli, M. Greco, and G. Martinelli, Nucl. Phys. B246 (1984) 12;
G. Altarelli, R.K. Ellis and G. Martinelli, Phys. Lett. 151B (1985) 457; Z. Phys. C27 (1985) 617
[24] UA1 collaboration, G. Arnison et al., Phys. Lett. 136B (1984) 294
[25] B.L. Combridge, J. Kripfganz and J. Ranft, Phys. Lett. 70B (1977) 234;
R. Cutler and D. Sivers, Phys. Rev. D17 (1978) 196;
J.F. Owens, E. Reya and M. Glück, Phys. Rev. D18 (1978) 1501
[26] J.C. Collins and D.E. Soper, Phys. Rev. D16 (1977) 2219
[27] V. Barger, A.D. Martin and R.J.N. Phillips, Phys. Lett. 125B (1983) 339, 343; Phys. Rev. D28 (1983) 145;
R.M. Godbole, S. Pakvasa and D.P. Roy, Phys. Rev. Lett. 50 (1983) 1539;
K. Hagiwara and W.F. Long, Phys. Lett. 132B (1983) 202;
V. Barger, H. Baer, A.D. Martin and R.J.N. Phillips, Phys. Rev. D29 (1984) 887;
V. Barger, H. Baer, K. Hagiwara, A.D. Martin and R.J.N. Phillips, Phys. Rev. D29 (1984) 1923
[28] UA1 collaboration, G. Arnison et al., Phys. Lett. 147B (1984) 493
[29] V. Barger, H. Baer, K. Hagiwara and R.J.N. Phillips, Phys Rev. D30 (1984) 947
[30] J. Cortés, K. Hagiwara and F. Herzog, Proc. 4th Topical Workshop on Proton-antiproton collider physics (Bern, 1984) p. 209
[31] A. Sirlin, Nucl. Phys. B192 (1981) 93